Remote Sensing of Environment 117 (2012) 322–337

Contents lists available at SciVerse ScienceDirect

Remote Sensing of Environment

journal homepage: www.elsevier.com/locate/rse

Fluorescence, temperature and narrow-band indices acquired from a UAV platform for water stress detection using a micro-hyperspectral imager and a thermal camera

P.J. Zarco-Tejada *, V. González-Dugo, J.A.J. Berni

Instituto de Agricultura Sostenible (IAS), Consejo Superior de Investigaciones Científicas (CSIC), Córdoba, Spain

ARTICLE INFO

Article history:
Received 24 May 2011
Received in revised form 5 October 2011
Accepted 6 October 2011
Available online 23 November 2011

Keywords:
Stress detection
Hyperspectral
Chlorophyll fluorescence
UAV
High resolution
Thermal

ABSTRACT

The remote detection of water stress in a citrus orchard was investigated using leaf-level measurements of chlorophyll fluorescence and *Photochemical Reflectance Index* (PRI) data, seasonal time-series of crown temperature and PRI, and high-resolution airborne imagery. The work was conducted in an orchard where a regulated deficit irrigation (RDI) experiment generated a gradient in water stress levels. Stomatal conductance (Gs) and water potential (Ψ) were measured over the season on each treatment block. The airborne data consisted on thermal and hyperspectral imagery acquired at the time of maximum stress differences among treatments, prior to the *re-watering* phase, using a miniaturized thermal camera and a micro-hyperspectral imager on board an unmanned aerial vehicle (UAV). The hyperspectral imagery was acquired at 40 cm resolution and 260 spectral bands in the 400-885 nm spectral range at 6.4 nm full width at half maximum (FWHM) spectral resolution and 1.85 nm sampling interval, enabling the identification of pure crowns for extracting radiance and reflectance hyperspectral spectra from each tree. The FluorMOD model was used to investigate the retrieval of chlorophyll fluorescence by applying the *Fraunhofer Line Depth* (FLD) principle using three spectral bands (FLD3), which demonstrated that fluorescence retrieval was feasible with the configuration of the UAV micro-hyperspectral instrument flown over the orchard. Results demonstrated the link between seasonal PRI and crown temperature acquired from instrumented trees and field measurements of stomatal conductance and water potential. The sensitivity of PRI and Tc–Ta time-series to water stress levels demonstrated a time delay of PRI vs Tc–Ta during the recovery phase after *re-watering* started. At the time of the maximum stress difference among treatment blocks, the airborne imagery acquired from the UAV platform demonstrated that the crown temperature yielded the best coefficient of determination for Gs ($r^2=0.78$; $p<0.05$) and Ψ ($r^2=0.34$; $p<0.001$). Among the narrow-band indices calculated, the PRI_{515} index (reference band = 515 nm) obtained better results than PRI_{570}, with $r^2=0.59$ ($p<0.01$) for Gs, and $r^2=0.38$ ($p<0.001$) for Ψ. The BGI1 index calculated from the blue (R_{400}) and green (R_{550}) bands resulted on the highest significance levels ($p<0.001$) for both Gs ($r^2=0.62$) and Ψ ($r^2=0.49$). Out of the structural indices assessed, RDVI, MTVI1 and TVI showed greater sensitivity for Gs ($r^2=0.6$; $p<0.01$) and Ψ ($p<0.001$) than NDVI. Chlorophyll fluorescence calculated from the micro-hyperspectral imagery with the FLD3 method tracked stress levels, obtaining $r^2=0.67$ ($p<0.05$) with stomatal conductance, and $r^2=0.66$ ($p<0.001$) with water potential. The work presented in this manuscript demonstrates the feasibility of thermal, narrow-band indices and fluorescence retrievals obtained from a micro-hyperspectral imager and a light-weight thermal camera on board small UAV platforms for stress detection in a heterogeneous tree canopy where very high resolution is required.

1. Introduction

Water deficits occur in plants when evaporative demand exceeds the supply of water in the soil (Slatyer, 1967). It has long been found that short-term water deficits may affect growth processes (Hsiao et al., 1976), and therefore early detection of water stress is important. Water stress also induces stomatal closure, which reduces the transpiration rate, thus decreasing evaporative cooling and increasing leaf temperature. The increase in leaf and canopy temperatures was first suggested in the 1960s as a method of tracking water stress using thermal infrared thermometers (Fuchs and Tanner, 1966; Idso et al., 1978; Idso et al., 1981; Jackson, 1982; Jackson et al., 1977a, 1977b; Jackson et al., 1981; Tanner, 1963). More recently, Sepulcre-Cantó et al. (2006, 2007) demonstrated that high-resolution airborne thermal imagers flown over orchard crops detected small canopy temperature differences linked to water stress levels. Later, Berni et al. (2009a) generated maps of tree canopy conductance (G_c) in orchards by applying a model based on canopy temperature

* Corresponding author at: Instituto de Agricultura Sostenible (IAS), Consejo Superior de Investigaciones Científicas (CSIC), Alameda del Obispo, s/n, 14004-Córdoba, Spain. Tel.: +34 957 499 280, +34 676 954 937; fax: +34 957 499 252.
E-mail address: pzarco@ias.csic.es (P.J. Zarco-Tejada).
URL: http://quantalab.ias.csic.es (P.J. Zarco-Tejada).

0034-4257/$ – see front matter © 2011 Elsevier Inc. All rights reserved.
doi:10.1016/j.rse.2011.10.007

estimated from high resolution airborne imagery, using as inputs net radiation and aerodynamic resistance as a function of wind speed and canopy structure.

Nevertheless, monitoring of plant water status is critical not only for early detection of stress, but also to enable the application of deficit irrigation (DI) techniques (Fereres and Soriano, 2007) with the degree of precision needed. Generally, when DI methods are correctly applied in many fruit tree species, yield and fruit size are not affected (Girona, 2002), while some quality parameters are increased and water is saved (Crisosto et al., 1994; Fereres and Soriano, 2007; Girona et al., 2003; Mills et al., 1994).

Even though canopy temperature is considered reliable as a proxy for plant water status monitoring (Jackson, 1982), there are physiological and remote sensing operational issues that support the development of new water-stress sensitive indices based on the visible and near infrared spectral regions (Suárez et al., 2009, 2010). On the physiology side, in some crop plants the diurnal patterns of stomatal conductance are such that the relationships between canopy temperature and stress levels are not clear-cut. This is the case of citrus trees in semi-arid areas, where high vapor pressure deficits induce a continuous decline in leaf conductance from the early morning hours, even when trees are well supplied with water (Fereres et al., 1979; Hall et al., 1975; Villalobos et al., 2008). The level of stomatal conductance thus interacts with the evaporative demand and internal water status of the tree to determine tree canopy temperature. On the operational side, monitoring of large agricultural fields of tree and vineyard crops, generally planted in grids and therefore affected by soil background and shadows, requires high spatial resolution and short revisit periods (Berni et al., 2009b). The satellite thermal imagery currently available is limited to Landsat TM and ASTER sensors, yielding 120 m and 90 m, respectively. In such cases, monitoring of water stress is potentially suitable for regional scales only when canopy heterogeneity is accounted for (Moran et al., 1994). Nevertheless, modeling methods conducted with DART 3D simulation for orchards demonstrated the large effects due to soil and shadow components on the aggregated thermal pixel as a function of planting grid and soil temperature variations (Sepulcre-Cantó et al., 2009), making it difficult to monitor stress levels even for the extreme conditions in discontinuous orchards.

Two *pre-visual* indicators of water stress proposed in the literature are the *Physiological Reflectance Index* (PRI) (Gamon et al., 1992), an index sensitive to the epoxidation state of the xanthophyll cycle pigments and to photosynthetic efficiency, serving as a proxy for water stress detection (Peguero-Pina et al., 2008; Suarez et al., 2008, 2009, 2010; Thenot et al., 2002), and the solar-induced chlorophyll fluorescence emission (Flexas et al., 1999, 2000, 2002; Moya et al., 2004) due to the link demonstrated between *steady-state* chlorophyll fluorescence and stomatal conductance. Although PRI was initially proposed as an indicator of the de-epoxidation state of the xanthophyll pigments and related to photosynthesis, recent studies demonstrate the sensitivity of this index for vegetation stress detection (Peguero-Pina et al., 2008; Suárez et al., 2009, 2010, 2008; Thenot et al., 2002). Therefore, PRI could be used for water stress detection as an alternative to thermal measurements, enabling the use of high spatial resolution capabilities that are more difficult in the thermal region.

The other pre-visual water stress indicator is chlorophyll fluorescence, as several studies demonstrated its link with photosynthesis and other plant physiological processes (Krause and Weis, 1984; Larcher, 1994; Lichtenthaler, 1992; Lichtenthaler and Rinderle, 1988; Papageorgiou, 1975; Schreiber and Bilger, 1987; Schreiber et al., 1994). Steady-state chlorophyll fluorescence (Fs) has received less attention than other fluorescence measures, but its potential as a physiological indicator of stress using remote sensing methods has been recently emphasized (Soukupová et al., 2008), along with increasing scientific interest during the past five years. Nevertheless, retrieval of the fluorescence signal is very challenging since the contribution to the radiance signal is estimated to be about 2–3%. Several methods have been reported to extract the fluorescence signal at the leaf and canopy levels (Meroni et al., 2004, 2008a, 2008b, 2009; Moya et al., 2004), which demonstrated the feasibility of fluorescence retrieval using the O_2-A band feature. Additional experiments conducted at 0.065 nm FWHM resolution using ratios between the 757 nm (*out*) and 760 nm (*in*) bands (Pérez-Priego et al., 2005) showed good diurnal relationships between fluorescence and water stress levels at the canopy scale.

Nevertheless, little work has been conducted for validation purposes at the airborne scale due to the lack of appropriate imagery at high spatial and spectral resolutions. Recent work (Zarco-Tejada et al., 2009) applied the *in-filling* method to 1 nm FWHM multispectral imagery acquired over peach, orange and olive orchards for water and nutrient stress detection. A thorough review of fluorescence detection methods can be found in Meroni et al. (2009), where the methodologies for fluorescence retrieval as a function of the type of instrument and number of bands available are discussed. Along these research objectives, a recent study assessed the impact of spectral sensor configurations on the *Fraunhofer Line Depth* (FLD) retrieval accuracy (Damm et al., 2011). A modeling work was used to study the effects of the spectral sampling interval, spectral resolution, signal to noise ratio, and spectral shift on the accuracy of the Fs retrievals using three FLD methods available. Results indicated the superior performance of the FLD3 method, the critical impact of the signal to noise ratio of the instrument used, and the feasibility for F retrievals with sensor configurations of 5 nm spectral resolution and small sampling intervals.

Although PRI, fluorescence and canopy temperature have been proposed for water stress detection, their use has not been assessed over an entire season. In addition, the sensitivity of both temperature and PRI measured at the tree crown level needs further study, including an assessment for a new index formulation for PRI using the 515 nm wavelength as a reference band (Hernández-Clemente et al., 2011). The research reported here used continuous leaf and crown measurements of temperature and PRI during a citrus experiment to assess the seasonal variations in water stress levels. In addition, a micro-hyperspectral imager and a thermal camera were installed on board an unmanned aerial vehicle (UAV), and the imagery used to extract pure crown temperature, radiance and reflectance spectra to estimate chlorophyll fluorescence, visible ratios and structural indices for water stress detection. The *Vegetation Fluorescence Canopy Model*

Table 1
Summary of each study site, ground data collected, and imagery acquisition dates. The treatments under RDI had a *withheld period* (no irrigation) followed by a re-watering period until their stem water potential was equal to the control.

Species	Treatments	Irrigation strategy	Withheld period	Irrigation dose	Continuous monitoring	During flights (09/14)
Mandarin	Field	Sustained			Ψ, Gs	
	100ET	Full requirements		100% ET	Leaf and canopy PRI, Tc, Ψ, Gs	
	RDI1	Regulated	06/23 to 08/31	37% ET during RDI period, later: 100% ET	Leaf and canopy PRI, Tc, Ψ, Gs	
	RDI2	Regulated	06/23 to 08/31	50% ET during RDI period, later: 100% ET	Ψ, Gs	
Orange	Field	Sustained			Ψ, Gs	Ψ
	100ET	Full requirements		100% ET	Tc, Ψ, Gs	Ψ, Gs
	RDI1	Regulated	06/23 to 09/15	37% ET during RDI period, later: 100% ET	Tc, Ψ, Gs	Ψ, Gs
	RDI2	Regulated	06/23 to 09/15	50% ET during RDI period, later: 100% ET	Ψ, Gs	Ψ

(FluorMOD) (Miller et al., 2004), a linked leaf model FluorMODleaf (Pedrós et al., 2004, 2008), and a canopy model FluorSAIL (Verhoef, 2004) were used to simulate canopy fluorescence and scattered radiance. Although the model requires further validation and refinement, FluorMOD was used as a tool for understanding the effects of the spectral bandwidth of the airborne sensor used to image the orchard for the retrieval of fluorescence through the FLD method.

2. Materials and methods

Field measurements were carried out during the 2010 irrigation season (from June through October) in a commercial citrus orchard, including leaf stomatal conductance (Gs), water potential (Ψ), and continuous point measurements of crown temperature and PRI. High resolution thermal and hyperspectral imagery was collected over the citrus orchard in September 2010 to assess the sensitivity of vegetation indices and canopy temperature for water stress detection.

2.1. Field experiments and airborne campaigns

2.1.1. Field data collection

The study was carried out in 2010 in two 0.6-ha plots of orange and mandarin trees in a commercial orchard located near La Campana, Seville (Spain) (37.8°N, 5.4°W). The orange trees (*Citrus sinensis* L. cv. Powell) were planted in 1997 in a 7 m × 4 m grid (358 trees/ha) in deep alluvial soil with a loam to sandy-loam texture. The mandarin (*Citrus reticulata* Blanco cv. Clemenvilla) orchard was planted in 1997 in a 7 m × 3 m grid. The climate in the area is Mediterranean, characterized by warm, dry summers and cool, wet winters, with an average annual rainfall and ETo (Penman–Monteith) of around 550 and 1300 mm, respectively.

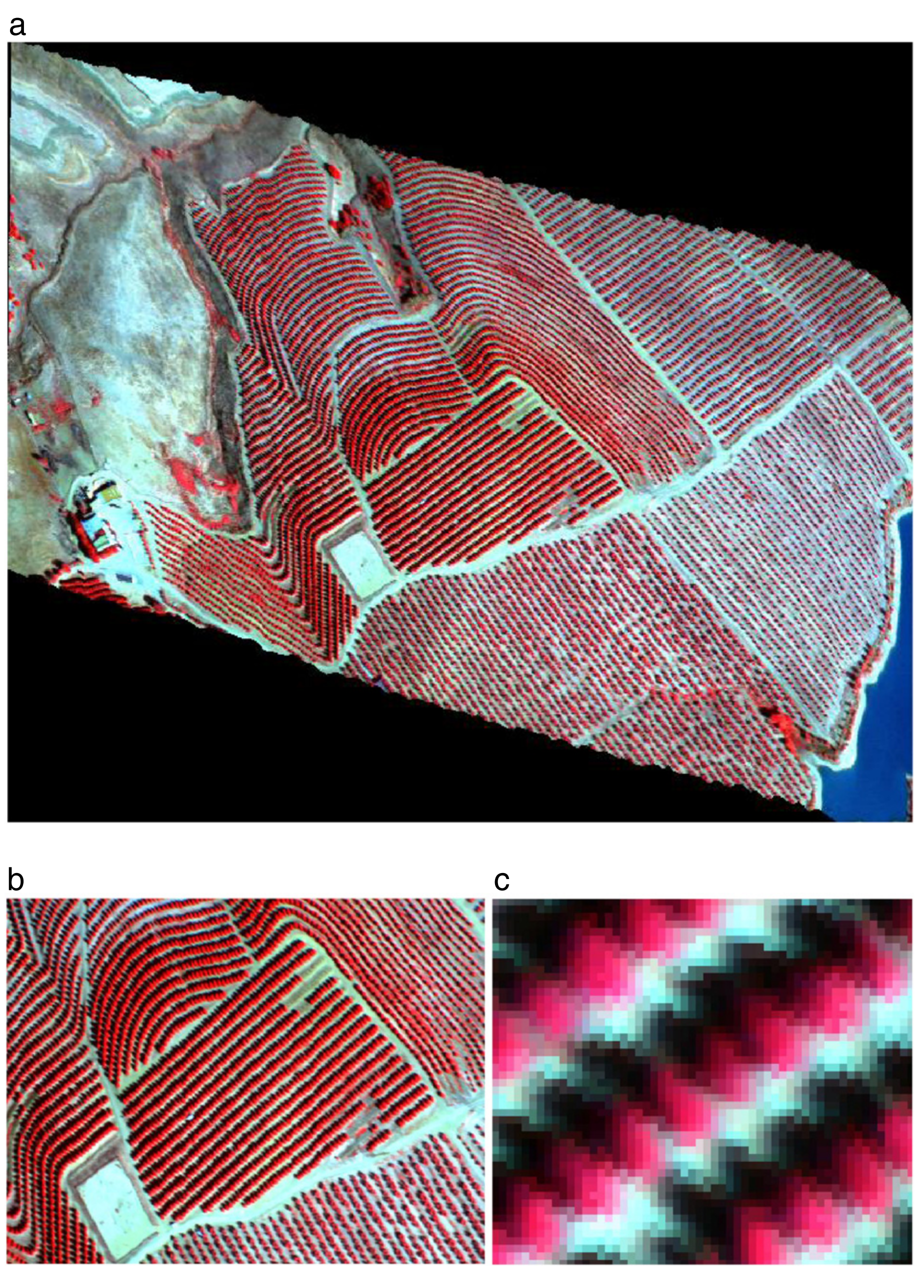

Fig. 1. Hyperspectral flight line acquired with the micro-hyperspectral imager on board the unmanned aerial vehicle (UAV) yielding 40 cm resolution and 260 spectral bands at 6 nm FWHM (a), observing the orchard study site used for field data collection (b) and the single tree identification due to the high resolution imagery acquired (c).

Four irrigation treatments were set up: i) farmer irrigation management (computed according to commercial practices); ii) 100% ET, where irrigation was scheduled to satisfy full (100%) ET requirements (estimated as crop evapotranspiration); iii) Regulated Deficit Irrigation (RDI1), with a deficit irrigation period (dates are shown in Table 1), where only 37% ET was applied; and iv) RDI2, similar to RDI1, but where the level of water application during the deficit irrigation period was 50% ET. Crop evapotranspiration was estimated as a crop coefficient (adapted to local conditions), and ETo was calculated from meteorological data provided by an automatic weather station located 10 km from the orchard. Each treatment was applied to individual plots of 12 trees and repeated four times. Table 1 lists the treatments, irrigation periods and depths, ground data collection and harvest and imagery acquisition dates for the orchard used in this study. Over the growing season, a Scholander pressure bomb (PWSC Model 3000, Soilmoisture Equipment Corp., CA, USA) was used to measure xylem water potential (Ψ) weekly or biweekly around noon on 4 selected trees per treatment. Stomatal conductance was measured on 12 trees using a leaf porometer (model SC-1, Decagon Devices, Inc., Pullman, WA, USA) at the time of the flights. On the same day, the number of water potential measurements was increased to a total of 40 monitored trees, representing a wide range of water stress conditions.

Leaf chlorophyll fluorescence measurements made under natural light conditions were conducted using the *Pulse-Amplitude-Modulated Fluorometer* PAM-2100 (Heinz Walz GMBH, Effeltrich, Germany), measuring steady-state Fs fluorescence on 8 selected trees, 30 leaves/tree. Fluorescence measurements were conducted at three times over the course of the day from 9.00 h until 15:00 h local time in order to monitor the diurnal variation of Fs for well-watered and water-stressed trees. Leaf PRI measurements calculated as $(R_{570}-R_{531})/(R_{531}+R_{570})$ (Suarez et al., 2008, 2009, 2010) were conducted on 4 mandarin trees (two trees under 100% ET irrigation treatment, and two RDI1 water-stressed trees), measuring each date 30 leaves/tree with a PlantPen instrument (Photon Systems Instruments, Brno, Czech Republic) for a total of 9 days from June until late September. Leaf PRI measurements were conducted between 11.00 h and 12.00 h local time on each date.

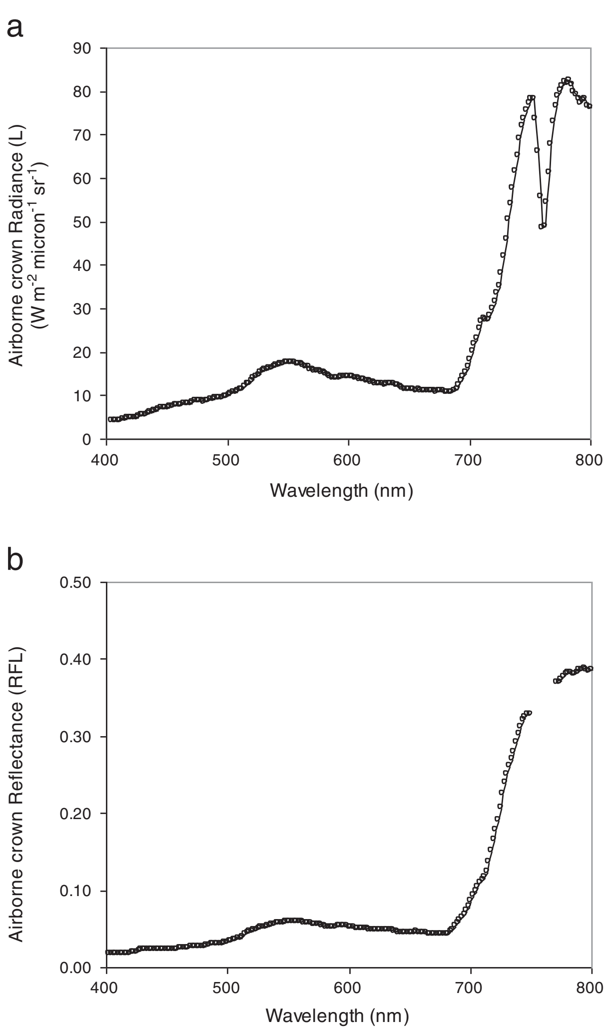

Fig. 2. Sample extraction of the mean crown radiance (a) and reflectance (b) for the 260 spectral bands at 6 nm FWHM acquired over the orchard.

In addition to the single-date measurements conducted for water potential, stomatal conductance, steady-state chlorophyll fluorescence, and leaf PRI, a total of 8 trees were instrumented with IRR-P thermal sensors (22° half-angle FOV) (Apogee, UT, USA) and 4 canopy PRI sensors (25° FOV) (SKR 1800, Skye Instruments, Powyd, UK), acquiring continuous thermal and PRI crown data (calculated as $(R_{570}-R_{531})/(R_{570}+R_{531})$) from May 2010 throughout the entire season in the mandarin and orange orchards. The multispectral Skye sensors were installed in tandem with the IRR-P thermal sensors, both targeting the same crown spots and acquiring at 530 and 570 nm bands with a 10 nm FWHM bandwidth. An additional PRI sensor was installed in the field for continuous measurement of downwelling irradiance using a cosine diffuser. The measurements were acquired at a rate of 1/s and were aggregated to store the mean value at 5-minute intervals in dataloggers installed in the field (model CR10X, Campbell Sci., UT, USA). Air temperature (T_a) data were measured continuously in the field with a Vaisala Weather Transmitter (model WXT510, Vaisala Oyj, Helsinki, Finland) installed in the study site 1 m above the trees.

The single-band infrared temperature (IRT) sensors covered the 6.5-14 μm range, and were assessed both in the laboratory and under natural sun conditions to characterize the IRT response to diurnal temperature variation (Sepulcre-Cantó et al., 2006), yielding errors within the accuracy limits of the instrument, ±0.4 °C, over a 5 °C to 40 °C range. All upwelling and downwelling instruments were calibrated in the laboratory using a uniform calibration body (integrating sphere, CSTM-USS-2000C Uniform Source System, LabSphere, NH, USA) at two different levels of illumination. Additionally, a radiance calibration was conducted at noon twice on each of the four upwelling PRI sensors using three lambertian panels of 2% (black), 50% (gray) and 98% reflectance (white) (LabSphere, NH, USA). The aim was to ensure a proper radiance calibration over the season and to test the linearity of the instruments under natural light conditions.

2.1.2. Airborne campaigns

An *unmanned aerial vehicle* (UAV) platform for remote sensing research was developed at the *Laboratory for Research Methods in Quantitative Remote Sensing* (QuantaLab, IAS-CSIC, Spain) to carry a payload with thermal and hyperspectral imaging sensors (Berni et al., 2009b; Zarco-Tejada et al., 2008). The UAV consisted of a 5-m wingspan fixed-wing platform capable of carrying a 3 kg payload for 1.5 h endurance at 13.5 kg take-off weight (TOW) (Viewer, ELIMCO, Seville, Spain). The UAV was controlled by an autopilot for autonomous flight (AP04, UAV Navigation, Madrid, Spain) to follow a flight plan using waypoints. The autopilot consists of a dual CPU controlling an integrated *Attitude Heading Reference System* (AHRS) based on a L1 GPS board, 3-axis accelerometers, yaw rate gyros and a 3-axis magnetometer (Berni et al., 2009b). Communication with the ground was conducted through a radio link where position, attitude and status data were transmitted at 20 Hz frequency; this also acted as a communication link for the operation of remote sensing hyperspectral and thermal cameras on board the UAV.

The hyperspectral imager installed on board the UAV was a micro-hyperspectral camera (Micro-Hyperspec VNIR model, Headwall

Photonics, MA, USA) flown in the spectral mode of 260 bands at 1.85 nm/pixel at 12-bit radiometric resolution, yielding an FWHM of 3.2 nm with a 12-micron slit, and 6.4 nm with a 25-micron slit. Data acquisition and storage on board the UAV was set to 50 fps, and integration time was 18 ms. The current system operated by QuantaLab-IAS-CSIC (Spain) is capable of acquiring 320 bands in the 400-1000 nm region, although the campaign described here was flown with 260 bands in the 400–885 nm region due to storage and data rate limitations at the time of the campaign. The 8-mm optics focal length yielded an IFOV of 0.93 mrad, an angular FOV of 50°, obtaining a swath of 522 m at 53 × 42 cm resolution, resampled to 40 cm for a flight conducted at 575 m AGL altitude and 75 km/h ground speed. The airborne campaign over the orchard consisted on flightlines acquired in the solar plane at 11.00 am local time on September 14th 2010, acquiring both hyperspectral and thermal imagery.

The hyperspectral imager was radiometrically calibrated using coefficients derived from measurements made with a calibrated uniform light source (integrating sphere, CSTM-USS-2000C Uniform Source System, LabSphere, NH, USA) at four different levels of illumination and six different integration times. Hyperspectral imagery was atmospherically corrected using the total incoming irradiance at 1 nm intervals simulated with the SMARTS model developed by the National Renewable Energy Laboratory, US Department of Energy (Gueymard, 1995, 2001) using aerosol optical depth measured at 550 nm with a Micro-Tops II sunphotometer (Solar LIGHT Co., Philadelphia, PA, USA) collected in the study areas at the time of the flights. SMARTS computes clear sky spectral irradiance, including direct beam, circumsolar, hemispherical diffuse, and total on a tilted or horizontal plane for specified atmospheric conditions. The algorithms were developed to match the output from the MODTRAN complex band models within 2%, but using aerosol optical depth as input. The spectral resolution is 0.5 nm for the 280–400 nm region, 1 nm for the 400–1750 nm, and 10 nm for 1750–4000 nm spectral regions. This radiative transfer model has been previously used in other studies to perform the atmospheric correction of narrow-band multispectral imagery, such as in Berni et al. (2009b) and Suárez et al. (2010). The output irradiance at 0.5 and 1 nm spectral bandwidth from SMARTS has been used as a reference irradiance spectra for solar energy studies (Gueymard et al., 2002) and available at http://www.nrel.gov/ (Gueymard, 2005).

An inertial measuring unit (IMU) installed on board the UAV synchronized with the hyperspectral imager was used to ortho-rectify the imagery using PARGE (ReSe Applications Schläpfer, Wil, Switzerland) (Fig. 1a). The orchard study site used for field data collection can be seen in Fig. 1b. The high resolution hyperspectral imagery acquired over the orchard enabled single tree identification for field validation purposes (Fig. 1c), successfully separating pure crown from shaded and sunlit soil reflectance. Each single pure tree crown from the entire orchard was identified using automatic object-based crown-detection algorithms, enabling the extraction of average crown radiance (Fig. 2a) and reflectance (Fig. 2b) for the 260 spectral bands acquired over the entire orchard. Each extracted crown was labeled as a function of the water stress treatment block (Fig. 3a), and each single crown spectrum was used for the analysis conducted through crown-level vegetation index calculation (Fig. 3c).

The two central trees of each irrigation treatment block (a total of 32 trees) plus 8 additional selected trees (40 trees in total) were used for water potential measurements conducted on the date of the airborne flight over the orange study site, September 14, 2010. The data extracted from each single crown using the hyperspectral reflectance imagery were used to calculate indices related to: i) epoxidation state of the xanthophyll cycle (EPS); ii) chlorophyll a + b concentration; iii) blue/green/red ratio indices; iv) carotenoid concentration; and v) tree crown structure.

The xanthophyll pigment indices were the *Photochemical Reflectance Index* (PRI) calculated with the 570 nm band as a reference (PRI_{570}) (Gamon et al., 1992) and with the 515 nm band as

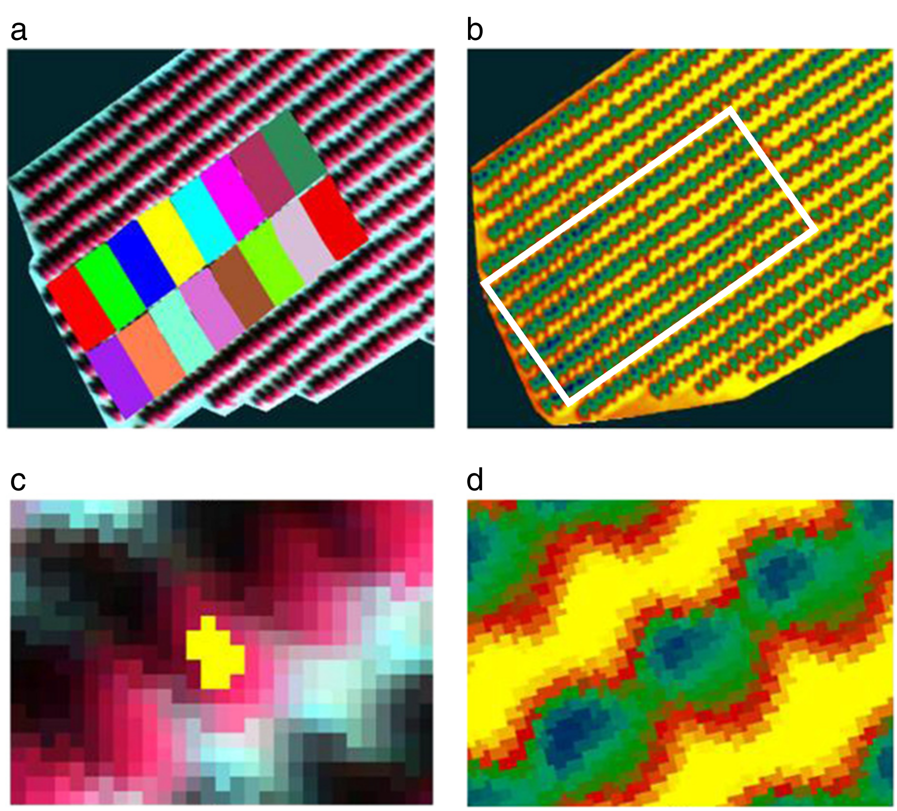

Fig. 3. Sixteen experimental irrigation blocks designed for well-watered (100%ET) and regulated deficit irrigation (RDI) schemes used for pure crown radiance and reflectance extraction (a) from the micro-hyperspectral imagery acquired at 40 cm resolution and 260 bands at 6 nm FWHM (c). The same experimental field was imaged using a high resolution thermal camera acquiring at 40 cm pixel size (b), enabling the extraction of pure tree crown temperature from each irrigation block (d).

a reference (PRI_{515}) shown to minimize structural effects (Hernández-Clemente et al., 2011). The chlorophyll a + b indices consisted of the R_{750}/R_{710} (ZM) (Zarco-Tejada et al., 2001), Vogelmann ($VOG1 = R_{740}/R_{720}$) (Vogelmann et al., 1993), and the family of indices based on the CARI index ($TCARI = 3*[(R_{700} - R_{670}) - 0.2*(R_{700} - R_{550})*(R_{700}/R_{670})]$) normalized by OSAVI ($(1+0.16)*(R_{800} - R_{670})/(R_{800} + R_{670} + 0.16)$) in the form suggested by Haboudane et al. (2002) (TCARI/OSAVI).

The blue/green/red ratio indices consisted of the Greenness index G (R_{550}/R_{670}), blue/green indices ($BGI1 = R_{400}/R_{550}$; $BGI2 = R_{450}/R_{550}$) (Zarco-Tejada et al., 2005) and blue/red indices ($BRI1 = R_{400}/R_{690}$; $BRI2 = R_{450}/R_{690}$), and the Lichtenthaler index ($LIC3 = R_{440}/R_{740}$) (Lichtenhaler et al., 1996). Other indices related to carotenoid concentration were calculated, including the R_{520}/R_{500}, R_{515}/R_{570}, and R_{515}/R_{670} (see Meggio et al., 2010; Hernández-Clemente et al., 2011, and Zarco-Tejada et al., 2005, for a full review of these indices).

Structural indices were calculated to assess if changes in the tree crown structure due to water stress could be captured by NDVI $(R_{800} - R_{670})/(R_{800} + R_{670})$ (Rouse et al., 1974), $RDVI = (R_{800} - R_{670})/\sqrt{(R_{800} + R_{670})}$ (Rougean and Breon, 1995), and other ratios such as the simple ratio SR (R_{800}/R_{670}) (Jordan, 1969), MSR ($\frac{R_{800}/R_{670} - 1}{(R_{800}/R_{670})^{0.5} + 1}$) (Chen, 1996), the OSAVI index, the triangular vegetation index $TVI = 0.5*[120*(R_{750} - R_{550}) - 200*(R_{670} - R_{550})]$ and the modified triangular index $MTVI1 = 1.2*[1.2*(R_{800} - R_{550}) - 2.5*(R_{670} - R_{550})]$ (see Haboudane et al., 2004, for a complete review of structural indices developed for robust estimation of LAI in crops).

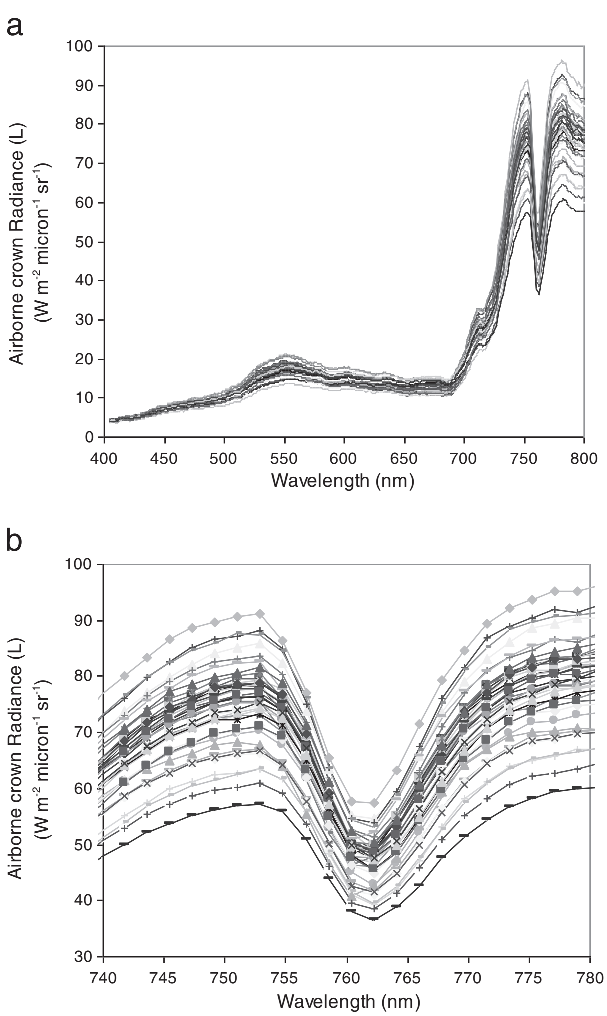

Fig. 4. Tree crown radiance spectra extracted from the 40 validation trees of the experiment at 40 cm resolution (a) used for fluorescence quantification with the 760 nm O_2-A FLD *in-filling* method. A total of 15 spectral bands at 6.4 nm FWHM within the O_2-A feature were acquired (b).

Radiance spectra for each single tree (Fig. 4a), later used for fluorescence retrieval at each tree crown using the 760 nm O_2-A *in-filling* method, were extracted (Fig. 4b) observing a total of 15 spectral bands within the O_2-A feature. Radiance difference and ratio indices based on the *in* (L762 nm) and *out* bands (L747 nm; L780 nm), the integral of the oxygen absorption between bands 747–780 nm, the curvature index (Zarco-Tejada et al., 2000), and the FLD methods using two (FLD2) and three (FLD3) spectral bands were applied to the hyperspectral imagery to estimate the fluorescence signal. A full review of methods to estimate the fluorescence signal using FLD and different spectral fitting methods can be found in Meroni et al. (2010).

The study area was also imaged with a thermal camera to derive surface temperature for each single crown under study (Fig. 3b). The thermal camera used was the Miricle 307 (Thermoteknix Systems Ltd., Cambridge, UK) equipped with a 14.25 mm f1.3 lens, connected to a computer via USB 2.0 protocol. The image sensor was a Focal Plane Array (FPA) based on uncooled microbolometers with a resolution of 640x480 pixels and a spectral response in the range of 8-12 µm, yielding a 25 µm pixel size. The camera delivered uncalibrated 14-bit digital raw images that were stored on board. Radiometric calibration was conducted in the laboratory using blackbodies under varying target and ambient temperatures to develop radiometric calibration algorithms. The sensor implemented an internal calibration for *non-uniformity correction* (NUC). Thermal images from the study area were acquired at 40 cm pixel resolution, enabling the retrieval of pure crown average temperature from each tree under study (Fig. 3d).

Atmospheric correction methods were applied to the thermal imagery based on the MODTRAN radiative transfer model to obtain surface temperature. Local atmospheric conditions were determined by air temperature, relative humidity and barometric pressure measurements at the time of flight using a portable weather station (Model WXT510, Vaisala, Finland) and were used as input into MODTRAN. Atmospheric correction methods conducted with single-band thermal cameras were shown to provide successful estimation of vegetation surface temperature (Berni et al., 2009b).

2.2. Modeling the fluorescence retrieval with FluorMOD

The standard retrieval of chlorophyll fluorescence through the *in-filling* method uses the canopy radiance (L) acquired from *fluorescing* (v) and *non-fluorescing* (n) targets *in* (i) and *out* (o) of the oxygen feature found at 760.5 nm, defined as L_i^v, L_i^n, L_o^v, L_o^n, respectively, to calculate the reflectance (R) and fluorescence (F) signals (Eqs. 1 and 2).

$$R = \frac{L_o^v - L_i^v}{L_o^n - L_i^n} \tag{1}$$

$$F = L_i^v - R \cdot L_i^n \tag{2}$$

This method was successfully tested at the leaf and canopy levels (Meroni et al., 2004, 2008a, 2008b; Moya et al., 2004) and also using subnanometer resolution at the canopy level for stress detection (Pérez-Priego et al., 2005). The application of this methodology at the image level (Maier et al., 2002; Zarco-Tejada et al., 2009) requires modeling approaches to understand the effects of the instrument spectral resolution and pixel size when aggregating fluorescing and non-fluorescing targets. The effects of the atmosphere are critical for the correct estimation of the absolute fluorescence signal. This is important because both the radiance extracted from pure tree crowns and the irradiance spectra are needed to calculate F, therefore being critical in multi-temporal or diurnal airborne campaigns under changing atmospheric conditions. In this study, the F retrieval for each tree crown was conducted under constant atmospheric conditions for all the monitored trees, playing the atmospheric effects a lower role.

The feasibility for estimating fluorescence with the hyperspectral imagery acquired as part of this study was assessed using the linked leaf-canopy fluorescence model developed as part of the FluorMOD project (Miller et al., 2004). FluorMODleaf (Pedrós et al., 2004) is a leaf fluorescence and reflectance model linked to FluorSAIL (Verhoef, 2004), a canopy reflectance and fluorescence model that simulates the fluorescence signal at the canopy level (detailed information on the linked leaf-canopy models can be found in Zarco-Tejada et al., 2006). In particular, the FluorMOD model was used in this study to assess the fluorescence retrieval FLD3 *in-filling* method (bands *in* L762 nm; *out* L747 nm and L780 nm) as a function of the spectral bandwidth of the hyperspectral instrument flown over the study sites in this study (see Zarco-Tejada et al., 2009, for simulations conducted to assess index sensitivity for fluorescence retrieval). A thorough modeling study conducted for a wide range of sensor configurations and FLD methods can be reviewed in Damm et al. (2011), which assessed the feasibility for F estimation as a function of the spectral sampling interval, spectral resolution, signal to noise ratio, and the spectral shift of the instrument used.

The inputs required to run the leaf and canopy model (Table 2) are the number of layers in PROSPECT (N); chlorophyll a + b content in μg/cm^2 (C_{ab}); water equivalent thickness in cm (C_w); dry matter content in μg (C_m); fluorescence quantum efficiency (Fi); leaf temperature in °C (T); species temperature dependence (S); and stoichiometry of PSII to PSI reaction centers (Sto). The canopy model requires the viewing zenith angle in degrees (Vza), relative azimuth angle in degrees (Raz), canopy leaf area index (LAI), hot spot parameter (h), and leaf inclination distribution function (LIDF).

The model was used to generate synthetic spectra through random input parameters such as fluorescence quantum efficiency F_i (0.03–0.06), chlorophyll content C_{ab} (30–80 μg/cm^2), and leaf area index LAI (2–4). FluorMOD modeled the leaf reflectance and transmittance spectra, along with the simulated fluorescence radiance for each reflectance and transmittance signal. The canopy fluorescence radiance (F) at 1 nm resolution was then simulated for each set of inputs (Fig. 5a), observing the canopy signal added to the canopy radiance as a function of the fluorescence amplitudes. The canopy radiance simulated at 1 nm resolution, which included the fluorescence effects (Fig. 5b), reproduced the peak depth at 760 nm used for fluorescence retrieval through the *in-filling* method (Fig. 5c). The similar spectral shape encountered both in the FluorMOD canopy radiance simulation in the 400–885 nm region and in the airborne hyperspectral imagery (Fig. 6a) shows the effects on the depth at 760 nm as a function of bandwidth (1 nm for the FluorMOD simulation; 6.4 nm for the hyperspectral imager flown over the study sites) (Fig. 6b).

The simulated canopy radiance spectra obtained with FluorMOD were spectrally resampled with a gaussian convolution to simulate the FWHM of the airborne hyperspectral imager. The 760 nm peak depth decreased as a function of bandwidth (Fig. 7), while still showing the feature as compared with the original 1 nm FWHM spectra. Such effects caused by the bandwidth were assessed by applying the FLD3 *in-filling* algorithm retrieval method to the FluorMOD simulated datasets. A comparison of the F retrieval as a function of the

Table 2
FluorMOD model inputs used in this study to assess the sensitivity of reflectance indices through atmospheric, leaf and canopy inputs. Parameters F_i, Cab and LAI were varied randomly within the range indicated in the table.

Atmospheric parameters			
Atmospheric	File	FLUORMOD30V23.MEP	
Irradiance	PAR dependence parameters: PARb = 0.0035; PARre = 0.005		
Visibility		23 km	
Solar zenith angle	30°		
Viewing zenith angle	0°		
Relative azimuth angle	0°		
Leaf inputs			
N	1.8	F_i	0.03–0.06
Cab	30–80 μg/cm^2	T	30 °C
Cw	0.025 cm	S	Standard
Cm	0.01 g/cm^2	Sto	1.5
Canopy inputs			
Leaf Area Index (LAI)	2–4		
LIDF parameter a	−0.5		
LIDF parameter b	−0.5		
Hot spot parameter	0.1		
Soil spectrum	Standard		

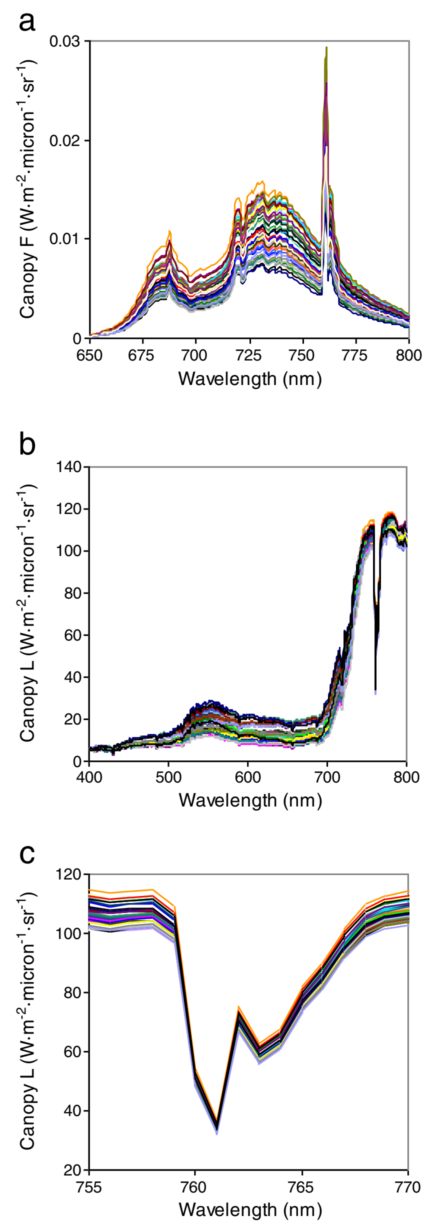

Fig. 5. Simulated canopy fluorescence radiance (F) at 1 nm resolution (a) and the canopy radiance including the fluorescence effects (b) using FluorMOD. The spectral range between 755 and 770 nm shows the peak depth at the 760 nm region used for fluorescence retrieval methods (c).

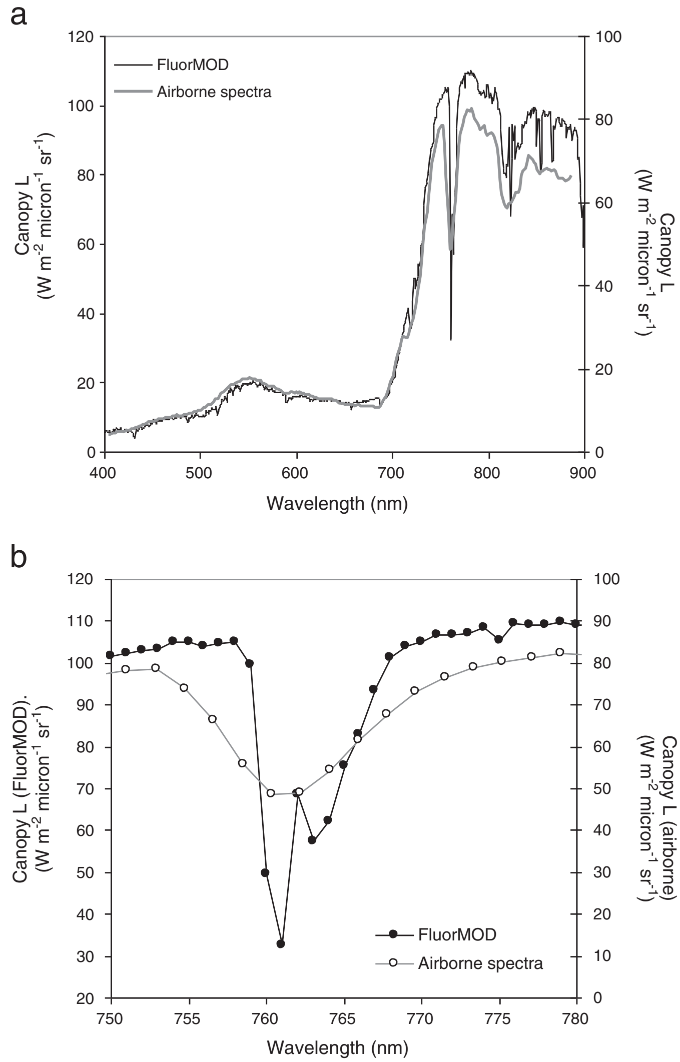

Fig. 6. Canopy radiance spectra simulated with FluorMOD in the 400–885 nm region as compared against the airborne micro-hyperspectral radiance extracted from a pure tree crown (a). Effects on the radiance depth at the 760 nm region as a function of bandwidth (1 nm for the FluorMOD simulation; 6.4 nm for the hyperspectral imager flown over the study sites) (b).

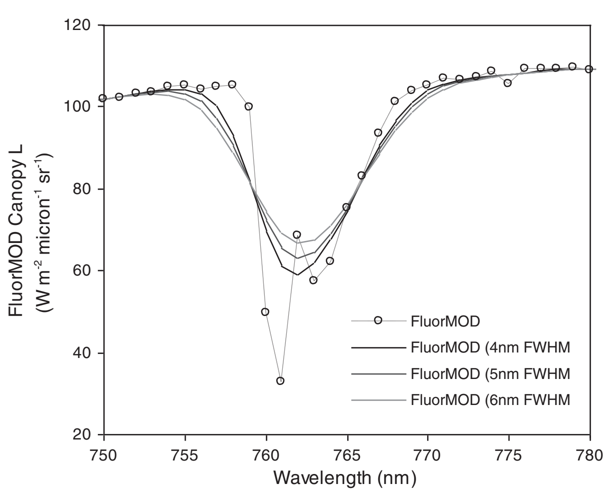

Fig. 7. Canopy radiance spectra simulated with FluorMOD (dotted line), and spectrally resampled through gaussian convolution to simulate the FWHM of the airborne hyperspectral imager (6 nm). The 760 nm peak depth decreases as a function of bandwidth, yet still showing the feature as compared with the original 1 nm FWHM spectra.

spectra bandwidth was conducted to assess if the 6.4 nm FWHM of the airborne hyperspectral imagery would enable retrieval of the fluorescence signal to allow the water stress detection sought in this study. The method to estimate the fluorescence signal from the FluorMOD simulated synthetic spectra consisted on the same FLD3 method applied to the airborne hyperspectral imagery, which used the *in* (L762 nm) and *out* bands (L747 nm; L780 nm) for the calculation. As previously indicated, the FLD3 method and others suitable depending on the spectral data available (number of bands and spectral bandwidth available) can be reviewed in Meroni et al. (2010).

3. Results

3.1. Modeling results conducted with FluorMOD

The synthetic spectra simulated from FluorMOD for varying fluorescence emissions (F_i), chlorophyll concentration (C_{ab}) and leaf area index values (LAI) showed good agreement for *R* (Eq. 1) ($r^2=0.99$; $p<0.001$) and *F* (Eq. 2) ($r^2=0.84$; $p<0.001$) when calculated with 1 nm and 6 nm FWHM spectral resolution. The close relationship between the *F* signal calculated at 1 and 6 nm bandwidth ($r^2=0.84$; $p<0.001$) demonstrated that the 6 nm spectra would still capture the input fluorescence emission. The absolute error obtained when comparing the *F* signal retrieved with the FLD3 *in-filling* method for both spectral resolutions against the fluorescence radiance signal simulated at 1 nm resolution (Fig. 8) yielded RMSE values of 4.58% (for the 1 nm FWHM spectra) and 12.16% (for the 6 nm FWHM spectra). The error increment obtained for the *F* retrieval (RMSE from 4.58% to 12.16%) as a function of the spectral resolution used, and the overall coefficient of determination obtained when using 6 nm FWHM spectra ($r^2 = 0.75$) suggests the potential retrieval of the fluorescence signal with larger spectral bandwidths and small sampling intervals when using the FLD3 method.

Further comparison between the estimated *F* signal through the FLD3 method and the FluorMOD inputs F_i, C_{ab} and LAI showed agreement between *F* and F_i ($r^2 = 0.8$; $p < 0.001$), and the lack of relationship between *F* and LAI ($r^2 = 0.01$; p-value not significant), and between F and C_{ab} ($r^2 = 0.05$; p-value not significant). These results demonstrate that the *F* signal retrieval using the FLD3 method is not correlated with C_{ab} and LAI. Moreover, it shows that a statistically significant relationship ($p < 0.001$) exists between fluorescence quantum efficiency and *F* estimation when conducted with 6 nm FWHM resolution spectra (12.16% RMSE). This is the spectral resolution of the airborne micro-hyperspectral imager used to fly over the sites in this study.

3.2. Experimental results

3.2.1. Leaf and crown measurement results

The diurnal leaf measurements conducted with the PAM-2100 fluorometer on attached leaves selected from well irrigated (100%ET) and deficit irrigation (RDI1) trees (Fig. 9a) showed lower steady-state fluorescence emission (Fs) for the water stressed trees during the experiment, as expected. The diurnal trend showed greater Fs differences between 100% ET and RDI1 in early morning than at noon. These results from citrus trees showing lower Fs values in RDI1 vs 100% ET irrigation levels coincide with the ones obtained in similar experiments in other crops, such as in olive and peach orchards under stress (Pérez-Priego et al., 2005; Zarco-Tejada et al., 2009).

The June–September time-series leaf PRI data (calculated as $(R_{570} - R_{531})/(R_{531} + R_{570})$) measured with the PlantPen instrument (Fig. 9b) show the seasonal trend for both 100% ET and RDI1 trees. Maximum differences in leaf PRI were found in July and August, corresponding to the times of maximum water potential differences among treatments (-0.98 and -1.73 MPa for 100% ET and RDI1 trees, respectively). The leaf PRI time series data showed the stress and recovery periods at the beginning and end of the irrigation experiment, with higher leaf PRI values measured for RDI1 than for the 100%ET, as expected. The well irrigated 100% ET trees showed a decline in PRI values from June (PRI = 0.046) until mid-July (PRI = 0.028), even though the water potential measured on the same trees was nearly identical ($\Psi = -0.84$ MPa in June, and $\Psi = -0.86$ MPa in July). Nevertheless, leaf PRI values measured on stressed trees were always higher than PRI values measured on 100% ET trees, in agreement with the work conducted by Suarez et al. (2008, 2009, 2010) in citrus and olive orchards. The seasonal variation of leaf PRI measurements could be due to changes in the xanthophyll epoxidation state over the season, but also due to potential effects caused by chlorophyll $a+b$, carotenoid and anthocyanin concentration as a function of the water stress. The leaf-level results obtained for Fs and PRI measured on stressed and well-watered trees had the intention to demonstrate that the results later obtained at canopy level were not caused by structural effects driven by water stress, but related to the physiological condition measured at the leaf level.

Results for the leaf PRI measurements obtained throughout the season are in agreement with canopy PRI, canopy Tc and the Tc–Ta data recorded with the Skye and Apogee sensors installed over 100% ET and RDI1 crowns (Fig. 10). The trends for PRI calculated as

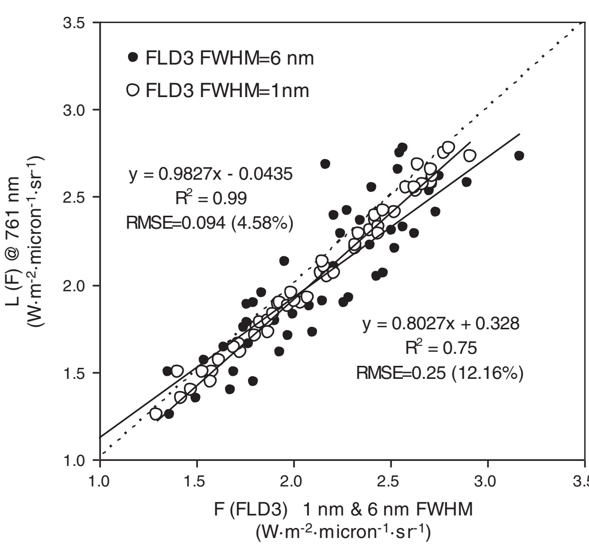

Fig. 8. Relationship obtained between the simulated FluorMOD fluorescence radiance and the fluorescence estimated (FLD3 method) from synthetic spectra at 1 nm (RMSE = 4.58%) and 6 nm FWHM (RMSE = 12.16%). RMSE values below 15% are found when using the spectral resolution (6.4 nm FWHM), sampling interval (1.85 nm) and signal to noise ratio (300:1 without binning) of the micro-hyperspectral imager used in this study.

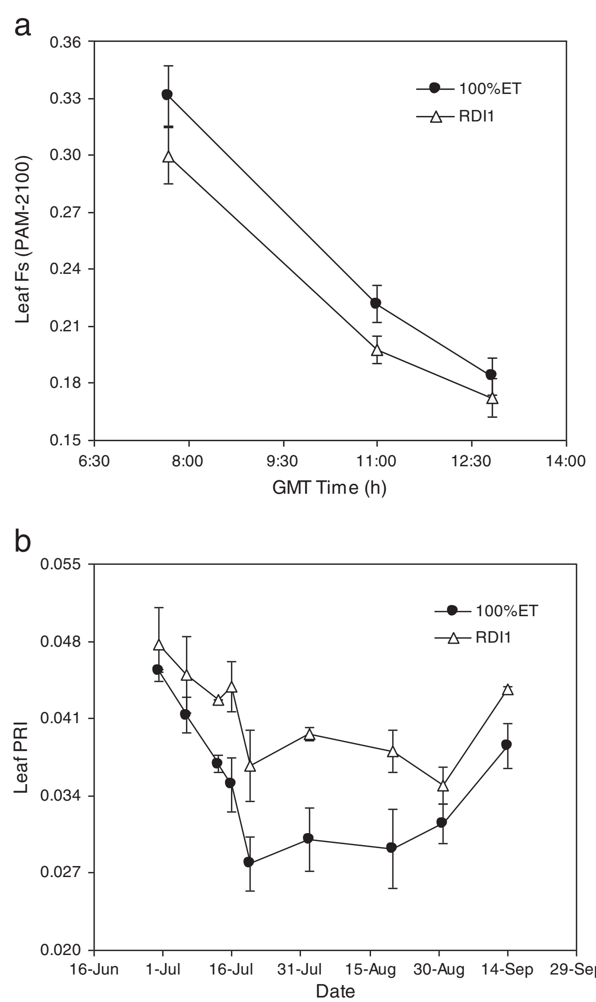

Fig. 9. (a) Diurnal mean leaf Fs values obtained with the PAM-2100 from trees under 100% ET (well-watered) and RDI (water-stressed) treatments (n = 30 per tree at each measuring time; error bars are the standard deviation); (b) mean leaf PRI measurements acquired from trees under 100% ET and RDI1 treatments over the course of the experiment, using the PlantPen instrument (n = 30 per tree at each measuring time; error bars are the standard deviation). PRI calculated as $(R_{570} - R_{531})/(R_{570} + R_{530})$.

$(R_{570}-R_{531})/(R_{570}+R_{531})$ and Tc–Ta measured at noon throughout the entire experiment demonstrate a similar seasonal pattern for both crown PRI and crown Tc–Ta on the RDI1 treatment (Fig. 10a). The time-series data indicate that both canopy PRI and Tc–Ta were coupled throughout the experiment, showing a maximum for both indicators at the time of the maximum stress ($\Psi = -1.73$ MPa; Tc–Ta = 5 K; PRI = −0.05), starting a recovery at the beginning of August when both Tc–Ta and PRI decreased together until the re-watering phase in mid-September. Although the general pattern for both indicators seemed similar throughout the experiment (Fig. 10a), a delay is observed on the PRI trend as compared against Tc–Ta: during the re-watering phase the crown temperature reaches Tc–Ta = 0 while PRI still shows values that indicate stress levels (PRI = −0.1). Therefore, the re-watering phase was first tracked by Tc–Ta, followed later by PRI. These results are consistent with the hypothesis that canopy temperature is linked to transpiration rates, and therefore is more short-term sensitive to water stress than PRI, which is linked to the epoxidation state of the xanthophyll cycle pigments. In addition to the indicated biochemical effects on leaf PRI, crown structural changes over the course of the season would also have a role on the canopy PRI trends observed during stress and on the re-watering phase. The seasonal trend observed in the continuous PRI data acquired for the March–November time frame corresponds as well with seasonal changes of irradiance, air temperature and vapor pressure deficit (VPD) levels.

A close look at the re-watering phase (Fig. 11) shows the behavior of canopy PRI and Tc–Ta acquired for two RDI1 trees as compared against a 100% ET reference tree. The patterns found indicate that the canopy PRI values measured on RDI1 trees started to decline after re-watering began, intersecting the non-water stress baseline (100%ET) at mid November (Fig. 11a). The agreement between Tc–Ta measured on reference (100%ET) and deficit RDI1 trees (Fig. 11b) shows that the recovery after re-watering started was detected earlier than when using PRI as an indicator of water stress. By the end of October the Tc–Ta values for 100% ET and RDI1 were equal (Tc–Ta below 1 K).

The general pattern for the Tc–Ta and PRI data acquired throughout the experiment varied when targeting well-watered trees (100% ET). In such case, the Tc–Ta and PRI range of variation acquired throughout the experiment on 100% ET trees was much narrower than the values measured on RDI trees due to the reduced stress levels and small variation of stress during the experiment on 100% ET trees (Tc–Ta below 2 K for the 100% ET trees as compared to Tc–Ta values up to 5 K on the stressed RDI1 trees) (Fig. 10b). Moreover, the Tc–Ta and PRI data acquired on well-watered trees showed values related to non-stress levels during the course of the experiment, with Tc–Ta below 2 K and PRI values close to PRI = −0.15 at all times. This was due to the full ET irrigation doses applied which assured low water stress conditions throughout the experiment, as demonstrated by the water potential measurements conducted:

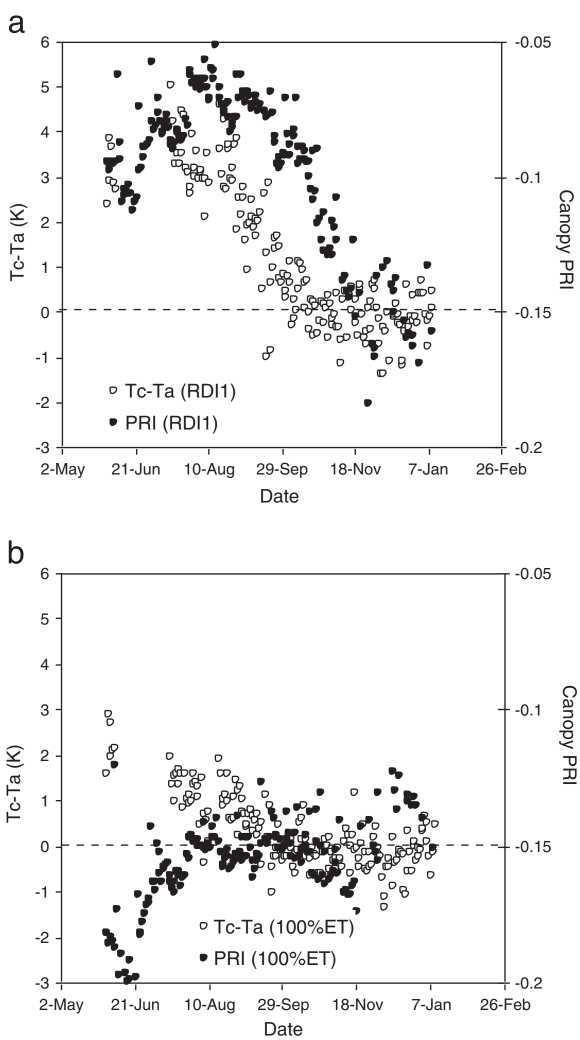

Fig. 10. Seasonal trends for canopy PRI and Tc–Ta (K) for RDI1 (a) and 100% ET (b) treatments acquired at noon (data shown are mean values for 5-minute intervals from measurements acquired at a rate of 1/s). PRI calculated as $(R_{570}-R_{531})/(R_{570}+R_{531})$.

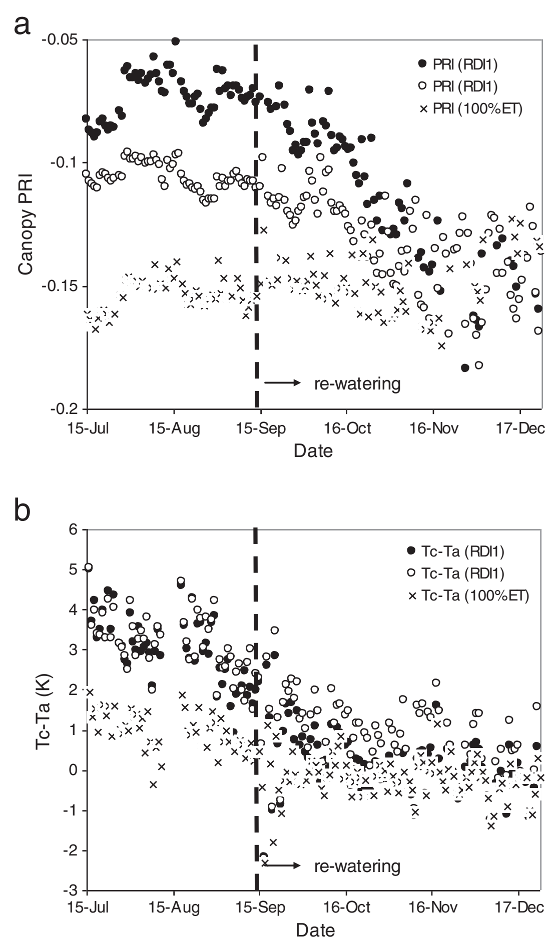

Fig. 11. Canopy PRI (a) and Tc–Ta (K) (b) obtained at noon from the stressed (RDI1) and well-watered (100%ET) irrigated trees over the course of the experiment. Plots show higher PRI and Tc–Ta values for the stressed (RDI1) trees (data shown are mean values for 5-minute intervals acquired at a rate of 1/s). PRI calculated as $(R_{570}-R_{531})/(R_{570}+R_{531})$.

mean $\Psi = -1.00$ MPa; maximum $\Psi = -0.73$ MPa; minimum $\Psi = -1.27$ MPa (while the variation of the RDI1 during the experiment ranged between $\Psi = -0.90$ MPa and $\Psi = -2.18$ MPa).

The water potential data measured on 100% ET and RDI1 trees over the entire experiment were compared against crown temperature and PRI (Fig. 12) to assess the seasonal trends during stress and recovery phases. The mid-day Tc and PRI canopy values for the dates when water potential measurements were made show an agreement between Tc and canopy PRI (Fig. 12a) and between water potential and PRI (Fig. 12b) for the RDI1 stressed trees. Therefore Figs. 12a and 12b show a similar trend for the remote sensing indicators (PRI, Tc) as compared with ground-measured water potential (Ψ). Nevertheless, Fig. 12b shows that the water potential decreases rapidly after re-watering (Ψ from -1.7 MPa down to -0.9 MPa in mid September) while canopy PRI decreased at lower rate over such re-watering phase. The data obtained on the well-watered trees (100%ET) showed a general lack of relationship between Tc and PRI (Fig. 12c) and between water potential and canopy PRI (Fig. 12d), probably due to the lower gradient found on the water potential measurements conducted over the season on the well-watered trees. These figures showed that the seasonal crown PRI and Tc–Ta data tracked water potential levels during the experiment, yielding coefficients of determination for PRI vs Ψ of $r^2 = 0.45$ ($p < 0.001$), and Tc–Ta vs Ψ of $r^2 = 0.44$ ($p < 0.001$).

3.2.2. Airborne hyperspectral and thermal imagery results

The hyperspectral and thermal airborne flights were conducted on September 14, prior to the re-watering phase, and therefore at the time of the maximum stress differences among treatment blocks. Based on the leaf water potential measurements observed (Ψ ranging from -0.5 to -2 MPa), the hyperspectral and thermal imagery acquired should be able to detect the stress levels measured in the field at the time of the flights. The high spatial resolution obtained in both hyperspectral and thermal imagery (40 cm resolution in both cases) enabled the identification of pure crowns (Figs. 1 and 3), enabling the comparison of tree-level water stress measurements and airborne-derived indices of stress.

The pure-crown temperature data extracted from the thermal imagery, and the narrow-band indices calculated from the hyperspectral imagery based on xanthophyll pigment absorption, chlorophyll a + b, blue/green/red ratios, carotenoid content, and structural indices were compared against the stomatal conductance and water potential measured at the time of the flights (Table 3). The best relationship with Gs was found for crown temperature ($r^2 = 0.78$; $p < 0.05$) (Fig. 13a). The reflectance indices calculated based on PRI formulations using R570 as the reference band (PRI_{570}) (Gamon et al., 1992) and the new formulation by Hernández-Clemente et al. (2011) (band R515 as reference to minimize structural canopy effects, PRI_{515}) yielded better performance for PRI_{515} ($r^2 = 0.59$; $p < 0.01$) than for PRI_{570} (p-value not significant) (Fig. 13c for PRI_{515}). This result confirms the findings by Hernández-Clemente et al. (2011) in forest canopies, which demonstrated the robustness of PRI_{515} to structural effects.

The chlorophyll indices TCARI and TCARI/OSAVI showed sensitivity to stress levels ($r^2 = 0.52$; $p < 0.05$ for TCARI), and the blue/green ratio BGI1 was highly significant ($r^2 = 0.62$; $p < 0.001$). The effects of water stress on the canopy structure were captured by structural indices such as RDVI ($r^2 = 061$; $p < 0.01$), TVI ($r^2 = 0.64$; $p < 0.01$) and MTVI ($r^2 = 0.66$; $p < 0.01$). These results for the structural indices are consistent due to the expected effects of sustained water stress on crown density.

The fluorescence retrieval conducted with the micro-hyperspectral imager showed that the best results were obtained for the FLD method

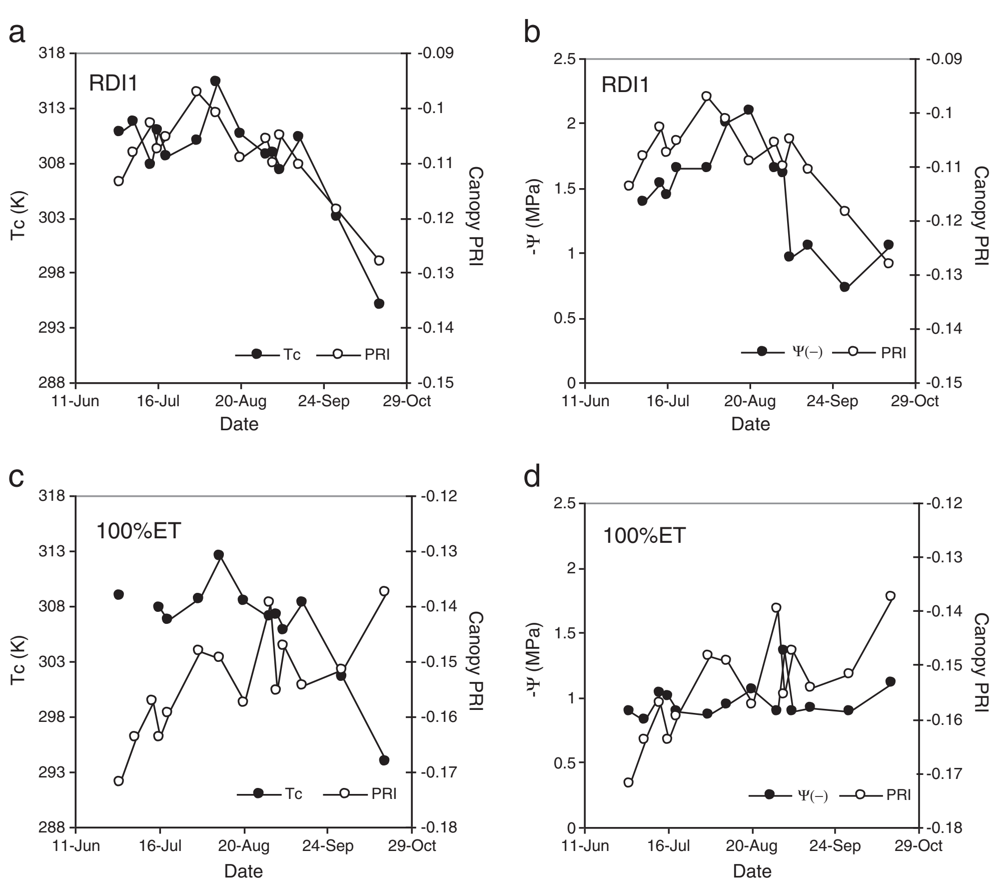

Fig. 12. Trends obtained for Tc (K) and PRI (a, c) as compared against water potential Ψ (MPa) (b, d) for the entire experiment, showing stressed (RDI1) (a, b) and well-watered (100%ET) (c, d) treatments. PRI calculated as $(R_{570} - R_{531})/(R_{570} + R_{531})$.

using two and three bands ($r^2=0.67$; $p<0.05$ for Gs) (Fig. 13e) as compared with radiance difference calculations and fluorescence integral methods. Radiance difference calculations L747 − L762 ($r^2=0.39$; p-value not significant), L780 − L762 ($r^2=0.55$; p-value not significant) and ((L747 + L780)/2)-L762 ($r^2=0.49$; p-value not significant) demonstrated lower performance than FLD2 and FLD3 methods ($r^2=0.67$; $p<0.05$). The ratio L747/L762 and L780/L762 were not related to the physiological measures Gs and Ψ ($r^2=0.05$; $r^2=0$, respectively; p-value not significant). The results obtained for the FLD2 and FLD3 methods were similar ($r^2=0.67$ for both methods; $p<0.05$), confirming the results presented in Damm et al. (2011) for instruments with short sampling intervals and FWHM around 5 nm. The curvature index calculated using bands 675, 682 and 690 nm yielded lower relationships, but statistically significant, for Gs ($r^2=0.47$; $p<0.05$) and Ψ ($r^2=0.51$; $p<0.001$) than when using the FLD2 and FLD3 methods.

The differences found in the coefficients of determination and the statistical significance between the remote sensing indicators of stress and Gs and Ψ (Table 3) are related to the stomatal regulation. The feedback of stomatal regulation on leaf water status has been observed in a number of cases, and results in the conservative behavior of water potential with increasing levels of water stress. In particular, this feedback mechanism between water potential and stomatal closure has been observed in deciduous trees (Fereres and Goldhamer, 1990) and in citrus (Fereres et al., 1979), and could affect the relationship between leaf water potential and other indicators of water stress. In particular, the relationships with water potential were highly significant for Tc ($r^2=0.34$; $p<0.001$) (Fig. 13b), PRI_{515} ($r^2=0.38$; $p<0.001$) (Fig. 13d), while the BGI1 index (blue/green ratio) yielded the highest significance level ($p<0.001$) for both Gs ($r^2=0.62$) and Ψ ($r^2=0.49$). The structural indices RDVI, MTVI1 and TVI, which obtained $r^2=0.6$ ($p<0.01$) for Gs, showed high significance with Ψ ($p<0.001$). Nevertheless, NDVI showed no significance with Gs and weaker sensitivity to Ψ ($r^2=0.24$; $p<0.01$). Chlorophyll fluorescence FLD3 retrievals demonstrated successful sensitivity to water stress, obtaining high statistical significance for both Gs and Ψ ($r^2=0.66$; $p<0.001$) (Fig. 13f).

The fluorescence retrievals obtained with the FLD3 method for the entire hyperspectral scene showed the spatial variability of the F signal from each single tree crown, and the differences detected between adjacent orchard fields (Fig. 14a). Within the experimental field, the fluorescence signal estimated from the two central trees of each treatment block was interpolated to generate a continuous fluorescence map of the experiment (Fig. 14b), enabling the visual comparison against the water potential map obtained from Ψ measurements conducted on each treatment (Fig. 14c).

Table 3
Coefficients of determination (r^2) obtained through temperature, narrow-band indices and fluorescence retrieval methods conducted with the hyperspectral radiance imagery as compared against stomatal conductance (Gs) and water potential (Ψ) measured at the time of the flights.

Airborne temperature, radiance and reflectance indices		Stomatal conductance and water potential	
		Gs	Ψ
Crown temperature (Tc)		0.78*	0.34***
Reflectance indices			
Xanthophyll indices	PRI_{570}	0.37	0.37***
	PRI_{515}	0.59**	0.38***
Chlorophyll a + b indices	ZM	0.26	0.02
	VOG1	0.29	0.02
	TCARI	0.52*	0.54***
	TCARI/OSAVI	0.45	0.51
Blue/green/red ratio indices	G	0.31	0.41***
	BGI1	0.62***	0.49***
	BGI2	0.48**	0.43***
	BRI1	0	0
	BRI2	0	0.04
	LIC3	0.34*	0.23**
Carotenoid indices	R_{520}/R_{500}	0.49**	0.48***
	R_{515}/R_{570}	0	0.05
	R_{515}/R_{670}	0.23	0.35***
Structural indices	NDVI	0.32	0.24**
	RDVI	0.61**	0.44***
	SR	0.33	0.23**
	MSR	0.33	0.23**
	OSAVI	0.52*	0.4***
	MTVI1	0.66**	0.49***
	TVI	0.64**	0.47***
Fluorescence indices			
$L_{747}-L_{762}$		0.39	0.46***
$L_{780}-L_{762}$		0.55	0.49***
L_{747}/L_{762}		0.05*	0
L_{780}/L_{762}		0	0
$((L_{747}+L_{780})/2)$-L_{762}		0.49	0.49***
FLD2 (747; 762)		0.67*	0.66***
FLD2 (780; 762)		0.67*	0.66***
FLD3 (747; 762; 780)		0.67*	0.66***
$\int$ [747,780]		0.62	0.6***
Curvature index		0.47*	0.51***

* $p<0.05$.
** $p<0.01$.
*** $p<0.001$.

4. Discussion

Several studies highlight the requirements for high spectral resolution instruments for the successful retrieval of chlorophyll fluorescence using subnanometer radiance data at the leaf (Meroni & Colombo, 2006) and canopy levels (Pérez-Priego et al., 2005). These studies demonstrated with experimental data that subnanometer spectral resolution spectrometers enabled the detection of steady-state fluorescence emission using the O_2-A absorption line for stress detection purposes. The interest on the very high spectral resolution was later supported in studies by Meroni et al. (2009, 2010) where a review on FLD and spectral fitting methods for the fluorescence retrieval as a function of the instrument configuration was conducted. Further, interest in spectral fitting methods as an alternative to FLD for F estimation with subnanometer spectral resolution increased under FLEX, FLuorescence EXplorer (European Space Agency, 2008), submitted to the European Space Agency (ESA) Earth Explorer program as a candidate algorithm for the scientific satellite mission concept. Along these efforts focused on the very high spectral resolution data, Zarco-Tejada et al. (2009) demonstrated that imaging chlorophyll fluorescence retrieval was feasible using 1 nm spectral resolution imagery acquired with a multispectral camera at 150 m altitude, using the 760.5 (*in*) and 757.5 nm (*out*) bands for the quantification of the solar-induced fluorescence at 15 cm pixel resolution. Other critical issues such as the assessment of the potential atmospheric effects were also investigated by Guanter et al. (2010).

Although these studies confirm the feasibility for fluorescence detection using very high spectral resolution data (under 1 nm FWHM), the operational issues related to the calibration and signal to noise ratio of the required instrument when acquiring at such narrow bandwidths may have important implications on the retrieval accuracy, cost and sensor availability for imaging purposes. In fact, these studies demonstrated the feasibility for fluorescence retrieval using very high spectral resolution (below 1 nm FWHM), but no published work using modeling and experimental data demonstrated the need for subnanometer radiance for accurate quantification of the fluorescence emission. The first modeling study assessing such requirements was recently published by Damm et al. (2011). In a modeling study using FluorSAIL3, they evaluated the F retrieval accuracy in response to the most relevant sensor properties, including the spectral sampling interval, spectral resolution, signal to noise, and the spectral shift, along with different fluorescence retrieval methods. This

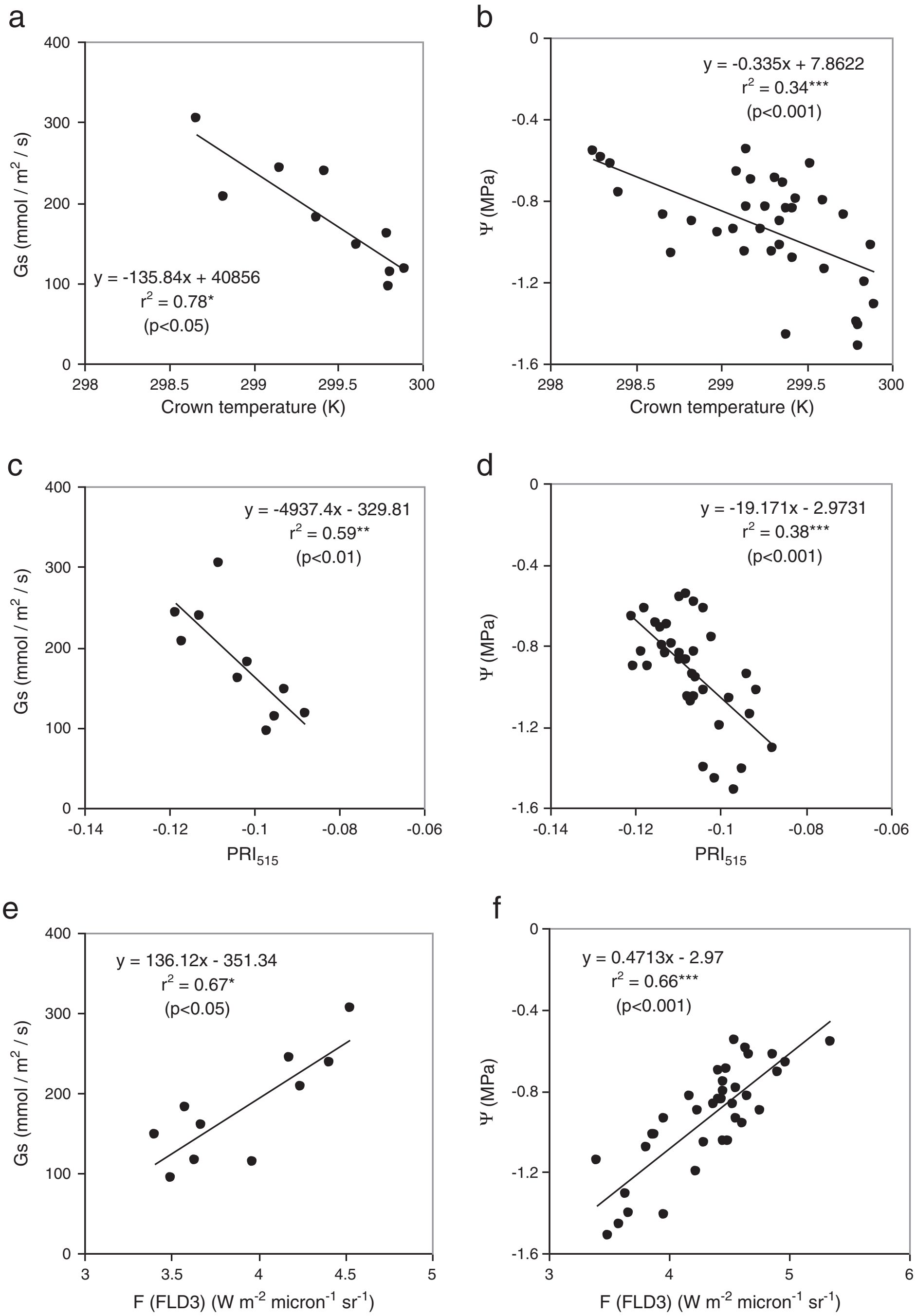

Fig. 13. Relationships obtained between airborne indices and ground truth data for Gs vs Tc (K) (a), PRI_{515} (c) and F (FLD3) (e), and against water potential (Ψ, MPa) (b, d, f).

relevant study demonstrated that the spectral resolution is important for the retrieval accuracy (up to 40% error was estimated as a function of the spectral resolution of the instrument), but the spectral sampling interval caused 12% error, and the spectral shift a 7% error. But more important, Damm et al. (2011) demonstrated that iFLD and FLD3 methods were able to retrieve the fluorescence signal when using lower spectral resolution (5 nm FWHM) and higher spectral sampling intervals (below 2.5 nm) with instruments with a minimum of 300:1 signal to noise ratio. These modeling results estimated an RMSE = 14% when a sensor configuration of 5 nm spectral resolution and a small sampling interval was used, and therefore are in agreement with the findings of this manuscript obtained with a micro-hyperspectral imager with 260 bands at 6 nm FWHM, 1.85 nm sampling interval (a total of 13 bands inside the O_2-A feature), and a signal to noise ratio of 300:1 without binning to target pure crowns affected by water stress. Furthermore, Damm et al. (2011) and this study demonstrate that subnanometer spectral resolution is not a requirement for F retrieval using the FLD3 method when high signal to noise ratio and short sampling intervals are used with bandwidths ranging 4–6 nm FWHM.

The work described in this manuscript used physiological indicators measured in the field, such as stomatal conductance and water potential, to assess if the fluorescence retrievals were in accordance with the expected stress levels of the experiment. The FLD3 method was conducted at the crown level, therefore removing the effects of shadows and soil, and estimating the fluorescence signal from pure vegetation pixels. Fluorescence emission quantities estimated in this manuscript were in agreement with other published work by Meroni

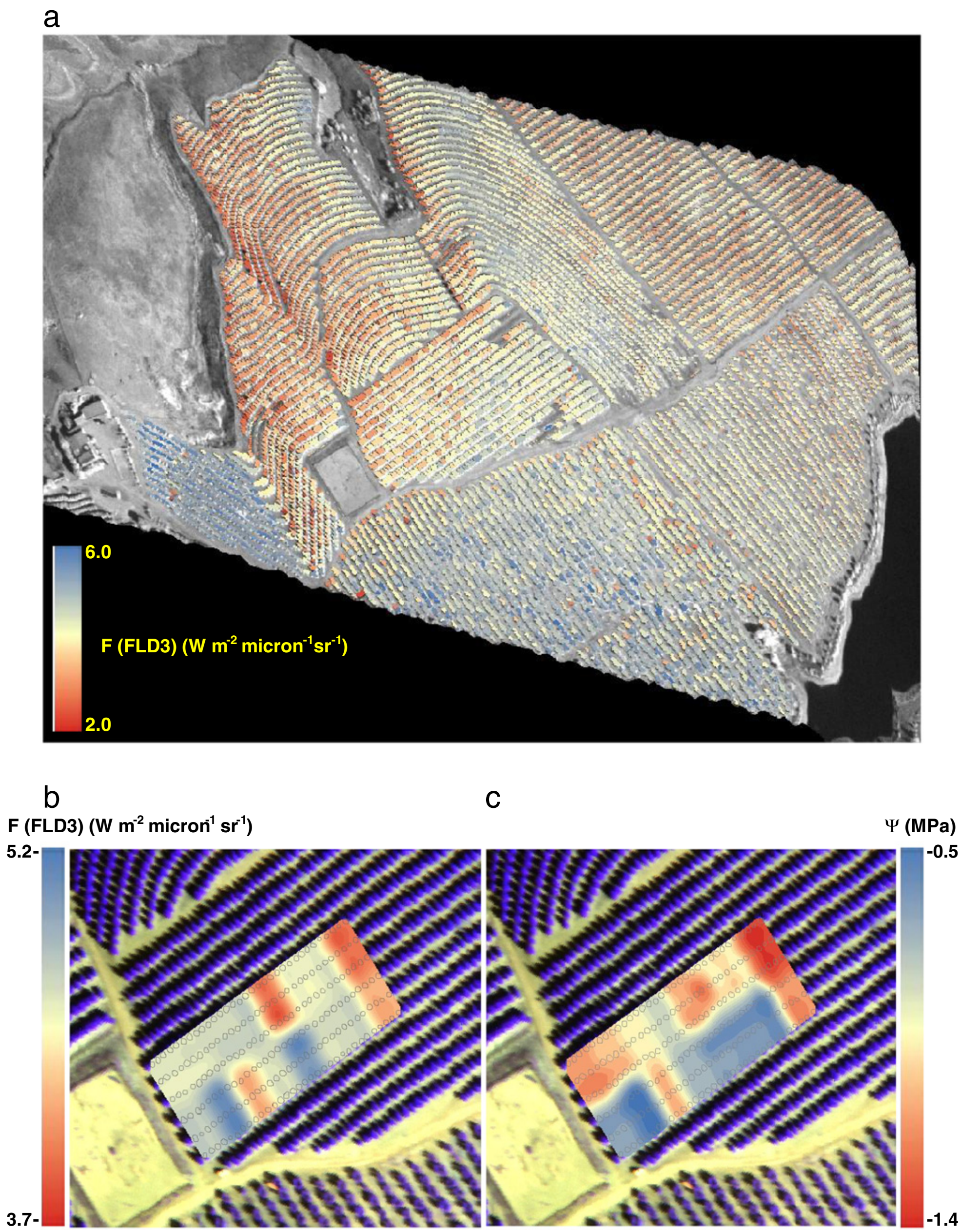

Fig. 14. Crown-level chlorophyll fluorescence maps obtained with the FLD3 method for the entire hyperspectral scene (a). Visual comparison between the fluorescence map of the experimental study area calculated from the two central trees of each treatment block (b) and the water potential measurements obtained from each irrigation block (c).

et al. (2009), Zarco-Tejada et al. (2009), and Damm et al. (2011). Studies such this one conducted with very high spatial resolution hyperspectral imagery (below 1 m pixel size) are needed for better understanding of the fluorescence signal retrieved from pure and mixed vegetation pixels, as well as for validating the available methods for fluorescence estimation. The work conducted with high resolution airborne imagery to target pure vegetation pixels is a first step required for understanding the fluorescence signal retrieved from different species and canopy structures. This is critical for making progress on the fluorescence estimation conducted from medium resolution instruments over aggregated pixels which include mixed vegetation, soil and shadows. In addition, the lack of fluorescence simulation models valid for non-homogeneous canopies prevents the assessment of the retrieval accuracy for validation studies under important targets such as forestry areas and cash crops like vineyards and tree orchards. The development of a model appropriate for open canopies will serve the scientific community to evaluate if the fluorescence retrieval under varying viewing geometries, direct soil contributions and percentage cover is feasible, as well as to better understand the fluorescence retrieval from mixed pixels. Finally, seasonal and diurnal measurements conducted over instrument targets (trees, lysimeters, study sites) with dedicated point-sensors will advance the knowledge related to the seasonal patterns in physiological indices widely used, such as temperature and reflectance indices for physiological monitoring through photosynthetic pigment absorption such as chlorophyll content, xanthophylls, carotenoids and anthocyanins. The recent work conducted using unmanned aerial vehicles and micro-hyperspectral imagers for remote sensing research (Berni et al., 2009b; Zarco-Tejada et al., 2008) bring new possibilities for extensive validation and experimental studies to make critical progress on fluorescence retrieval methods using unprecedented submeter hyperspectral imagery.

5. Conclusions

The work presented in this manuscript assessed thermal and multispectral domains for water stress detection in a citrus orchard. High resolution imagery acquired from a thermal camera and a micro-hyperspectral sensor on board an unmanned aerial vehicle enabled the identification of pure crowns, extracting the mean reflectance and temperature for individual trees where field measurements of stomatal conductance and water potential were measured. The experimental design comprised random blocks with full (100%ET), farmer irrigation method, and two deficit irrigation levels (RDI) offering a range of water stress levels.

The time series acquired from regulated deficit treatments (RDI1) and well irrigated blocks (100%ET) treatment trees instrumented with thermal and PRI point sensors demonstrated that both Tc–Ta and PRI crown data were able to track the seasonal variation of stress and recovery at the end of the experiment. The time series data demonstrated a time delay in the sensitivity of PRI as compared to Tc–Ta variation. To ensure that PRI did not solely track crown structural variation over the course of the experiment, leaf-level PRI measurements were also acquired, demonstrating that leaf PRI data were also linked to water potential levels throughout the season. Nevertheless, leaf biochemical and canopy biophysical effects on PRI over the course of the season would also affect the PRI indices used to track water stress levels.

The airborne flights conducted with a thermal camera and a micro-hyperspectral imager enabled water stress detection assessment by using crown temperature, narrow-band VIS–NIR formulations, and chlorophyll fluorescence. The simulation work conducted with the FluorMOD model for different spectral bandwidths demonstrated that the fluorescence signal retrieved through the FLD3 *in-filling* method was related to water potential and stomatal conductance measurements when 6 nm FWHM spectra was used. Among the different methods used to retrieve the fluorescence signal, including the radiance difference, the integral of the 760 nm peak, and the FLD2 and FLD3 methods, the sensitivity of fluorescence retrievals to water stress levels suggested that the FLD3 method using 747, 762 and 780 nm bands was the best method with 6 nm FWHM and 1.85 nm sampling spectra.

Among crown temperature, narrow-band indices, and fluorescence retrieval conducted from the airborne radiance spectra, the best indicators of water stress were crown temperature, chlorophyll fluorescence calculated with the FLD3 method, the PRI_{515} index (reference band = 515 nm), which was more sensitive to water stress than PRI_{570} (reference band = 570 nm) as in Hernández-Clemente et al. (2011) in forest canopies. The BGI1 index calculated from the blue (R_{400}) and green (R_{550}) bands yielded the highest significance level ($p<0.001$) for both Gs ($r^2=0.62$) and Ψ ($r^2=0.49$). Out of the structural indices assessed, RDVI, MTVI1 and TVI were related to Gs ($p<0.01$), obtaining high significance with Ψ ($p<0.001$), while NDVI showed no significance with Gs and a weak sensitivity to Ψ. Chlorophyll fluorescence calculated with the FLD3 method from the micro-hyperspectral imager demonstrated successful sensitivity to stress levels, yielding $r^2=0.67$ ($p<0.05$) with Gs, and $r^2=0.66$ ($p<0.001$) with water potential. The fluorescence estimations from the hyperspectral imagery were in agreement with ground measurements of fluorescence, which demonstrated lower values in water stressed trees.

The work presented in this manuscript demonstrated the ability to track stress levels in a citrus crop using thermal and hyperspectral imagery acquired with an unmanned aerial vehicle, showing that crown temperature, the blue-green BGI1 index, and the chlorophyll fluorescence estimates were the best related to water stress. Results confirmed previous work that showed the link between PRI and Tc, and the superior performance of PRI_{515} vs PRI_{570}. The use of lightweight micro-hyperspectral imagers and miniature thermal cameras on board UAV platforms will enable flexible and cost-effective data collection campaigns for precision agriculture and environmental applications in the near future.

Acknowledgments

Financial support from the Spanish Ministry of Science and Education (MEC) for the AGL2009-13105 and CONSOLIDER RIDECO (CSD2006-67) projects is gratefully acknowledged. M. Medina, D. Notario, A. Vera, A. Hornero, R. Romero, R. Gutierrez and P. Cidare are acknowledged for technical support during field and airborne campaigns. The editorial comments of E. Fereres are appreciated.

References

Berni, J. A. J., Zarco-Tejada, P. J., Sepulcre-Cantó, G., Fereres, E., & Villalobos, F. J. (2009). Mapping canopy conductance and CWSI in olive orchards using high resolution thermal remote sensing imagery. *Remote Sensing of Environment*, *113*, 2380–2388.

Berni, J. A. J., Zarco-Tejada, P. J., Suarez, L., & Fereres, E. (2009). Thermal and narrowband multispectral remote sensing for vegetation monitoring from an unmanned aerial vehicle. *IEEE Transactions on Geoscience and Remote Sensing*, *47*(3), 722–738.

Chen, J. (1996). Evaluation of vegetation indices and modified simple ratio for boreal applications. *Canadian Journal of Remote Sensing*, *22*, 229–242.

Crisosto, C. H., Johnson, R. S., Luza, J. G., & Crisosto, G. M. (1994). Irrigation regimes affect fruit soluble solids concentration and rate of water loss of "O'Henry" Peaches. *HortScience*, *29*(10), 1169–1171.

Damm, A., Erler, A., Hillen, W., Meroni, M., Schaepman, M. E., Verhoef, W., et al. (2011). Modeling the impact of spectral sensor configurations on the FLD retrieval accuracy of sun-induced chlorophyll fluorescence. *Remote Sensing of Environment*, *115*, 1882–1892.

European Space Agency (2008). *ESA SP-1313/4 candidate earth explorer core missions—Reports for assessment: FLEX-FLuorescence EXplorer*. Noordwijk, The Netherlands: ESA Communication Production Officehttp://esamultimedia.esa.int/docs/SP1313-4_FLEX.pdf available on line at

Fereres, E., Cruz-Romero, G., Hoffman, G. F., & Rawlins, S. L. (1979). Recovery of orange trees following severe water stress. *Journal of Applied Ecology*, *16*, 833–842.

Fereres, E., & Soriano, M. (2007). Deficit irrigation for reducing agricultural water Use. *Journal of Experimental Botany*, *58*, 147–159.

Fereres, E., & Goldhamer, D. A. (1990). Deciduous fruit and nut trees. In B. A. Stewart, & D. R. Nielsen (Eds.), *Irrigation of Agricultural Crops, Agronomy*, *30*. (pp. 987–1017) Madison, WI: ASA, CSSA, SSSA.

Flexas, J., Escalona, J. M., & Medrano, H. (1999). Water stress induces different levels of photosynthesis and electron transport rate regulation in grapevines. *Plant, Cell & Environment*, *22*, 39–48.

Flexas, J., Briantais, J. M., Cerovic, Z., Medrano, H., & Moya, I. (2000). Steady-state and maximum chlorophyll fluorescence responses to water stress in grapevine leaves: A new remote sensing system. *Remote Sensing of Environment*, *73*, 282–297.

Flexas, J., Escalona, J. M., Evain, S., Gulias, J., Moya, I., Osmond, C. B., et al. (2002). Steady-state chlorophyll fluorescence (Fs) measurements as a tool to follow variations of net CO2 assimilation and stomatal conductance during water-stress in C-3 plants. *Physiologia Plantarum*, *114*(2), 231–240.

Fuchs, M., & Tanner, C. B. (1966). Infrared thermometry of vegetation. *Agronomy Journal*, *58*, 297–601.

Gamon, J. A., Peñuelas, J., & Field, C. B. (1992). A narrow-wave band spectral index that tracks diurnal changes in photosynthetic efficiency. *Remote Sensing of Environment*, *41*, 35–44.

Girona, J. (2002). Regulated deficit irrigation in peach. *A global analysis, Acta Horticulturae*, *592*, 335–342.

Girona, J., Mata, M., Arbonès, A., Alegre, S., Rufat, J., & Marsal, J. (2003). Peach tree response to single and combined regulated deficit irrigation regimes under shallow soils. *Journal of the American Society of Horticultural Sciences*, *128*, 432–440.

Guanter, L., Alonso, L., Gomez-Chova, L., Meroni, M., Preusker, R., & Fischer, J. (2010). Developments for vegetation fluorescence retrieval from spaceborne high resolution spectrometry in the O_2-A and O_2-B absorption bands. *Journal of Geophysical Research-Atmospheres*, *115*.

Gueymard, C. A. (1995). SMARTS, a simple model of the atmospheric radiative transfer of sunshine: Algorithms and performance assessment. *Technical report no. FSEC-PF-270-95*. Cocoa, FL: Florida Solar Energy Center.

Gueymard, C. A. (2001). Parameterized transmittance model for direct beam and circumsolar spectral irradiance. *Solar Energy*, *71*(5), 325–346.

Gueymard, C. A., Myers, D., & Emery, K. (2002). Proposed reference irradiance spectra for solar energy systems testing. *Solar Energy*, *73*(6), 443–467.

Gueymard, C. A. (2005). *SMARTS code, version 2.9.5 user's Manual solar consulting services*. Online PDF document from http://www.nrel.gov/rredc/smarts/.

Haboudane, D., Miller, J. R., Tremblay, N., Zarco-Tejada, P. J., & Dextraze, L. (2002). Integrated narrow-band vegetation indices for prediction of crop chlorophyll content for application to precision agriculture. *Remote Sensing of Environment*, *84*, 416–426.

Haboudane, D., Miller, J. R., Pattey, E., Zarco-Tejada, P. J., & Strachan, I. (2004). Hyperspectral vegetation indices and novel algorithms for predicting green LAI of crop canopies: Modeling and validation in the context of precision agriculture. *Remote Sensing of Environment*, *90*(3), 337–352.

Hall, A. E., Camacho-B, S. E., & Kaufmann, M. R. (1975). Regulation of water loss by citrus leaves. *Physiologia Plantarum*, *33*, 62–65.

Hernández-Clemente, R., Navarro-Cerrillo, R. M., Suárez, L., Morales, F., & Zarco-Tejada, P. J. (2011). Assessing structural effects on PRI for stress detection in conifer forests. *Remote Sensing of Environment*, *115*(9), 2360–2375.

Hsiao, T. C., Fereres, E., Acevedo, E., & Henderson, D. W. (1976). *Water stress and dynamics of growth and yield of crops, water and plant life: Problems and modern approaches.* : Springer.

Idso, S. B., Jackson, R. D., & Reginato, R. J. (1978). Extending the "degree day" concept of phenomenological development to include water stress effects. *Ecology*, *59*, 431–433.

Idso, S. B., Jackson, R. D., Pinter, P. J., Reginato, R. J., & Hatfield, J. L. (1981). Normalizing the stress-degree-day parameter for environmental variability. *Agricultural and Forest Meteorology*, *24*, 45–55.

Jackson, R., Reginato, R., & Idso, S. (1977). Wheat canopy temperature: A practical tool for evaluating water requirements. *Water Resources Research*, *13*, 651–656.

Jackson, R. D., Idso, S. B., Reginato, R. J., & Ehrler, W. L. (1977). Crop temperature reveals stress. *Crop Soils*, *29*, 10–13.

Jackson, R. D., Idso, S. B., Reginato, R. J., & Pinter, P. J., Jr. (1981). Canopy temperature as a crop water stress indicator. *Water Resources Research*, *17*, 1133–1138.

Jackson, R. D. (1982). Canopy temperature and crop water stress. *Advances in Irrigation*, *1*, 43–85.

Jordan, C. F. (1969). Derivation of leaf area index from quality of light on the forest floor. *Ecology*, *50*, 663–666.

Krause, G. H., & Weis, E. (1984). Chlorophyll fluorescence as a tool in plant physiology. II. Interpretation of fluorescence signals. *Photosynthesis Research*, *5*, 139–157.

Larcher, W. (1994). Photosynthesis as a tool for indicating temperature stress events. In E. D. Schulze, & M. M. Caldwell (Eds.), *Ecophysiology of photosynthesis* (pp. 261–277). Berlin: Springer.

Lichtenthaler, H. K., & Rinderle, U. (1988). The role of chlorophyll fluorescence in the detection of stress conditions in plants. *CRC Critical Reviews in Analytical Chemistry*, *19*(Suppl. 1), 529–585.

Lichtenthaler, H. K. (1992). The Kautsky effect: 60 years of chlorophyll fluorescence induction kinetics. *Photosynthetica*, *27*, 45–55.

Lichtenhaler, H. K., Lang, M., Sowinska, M., Heisel, F., & Mieh, J. A. (1996). Detection of vegetation stress via a new high resolution fluorescence imaging system. *Journal of Plant Physiology*, *148*, 599–612.

Maier, S. W., Günther, K. P., & Stellmes, M. (2002). *Remote sensing and modelling of solar induced fluorescence, 1st workshop on remote sensing of solar induced vegetation fluorescence.* Netherlands: Noordwijk.

Meggio, F., Zarco-Tejada, P. J., Núñez, L. C., Sepulcre-Cantó, G., Gonzalez, M. R., & Martin, P. (2010). Grape quality assessment in vineyards affected by iron deficiency chlorosis using narrow-band physiological remote sensing indices. *Remote Sensing of Environment*, *114*, 1968–1986.

Meroni, M., Colombo, R., & Cogliati, S. (2004). High resolution leaf spectral signature for the detection of solar induced chlorophyll fluorescence. *Proceedings of the 2nd ESA workshop on remote sensing of solar induced vegetation fluorescence, Montreal, Canada, 17–19 November 2004*.

Meroni, M., & Colombo, R. (2006). Leaf level detection of solar-induced chlorophyll fluorescence by means of a subnanometer resolution spectroradiometer. *Remote Sensing of Environment*, *103*, 438–448.

Meroni, M., Picchi, V., Rossini, M., Cogliati, S., Panigada, C., Nali, C., et al. (2008). Leaf level early assessment of ozone injuries by passive fluorescence and PRI. *International Journal of Remote Sensing*, *29*(17), 5409–5422.

Meroni, M., Rossini, M., Picchi, V., Panigada, C., Cogliati, S., Nali, C., et al. (2008). Assessing steady-state fluorescence and PRI from hyperspectral proximal sensing as early indicators of plant stress: The case of ozone exposure. *Sensors*, *8*, 1740–1754.

Meroni, M., Rossini, M., Guanter, L., Alonso, L., Rascher, U., & Colombo, R. (2009). Remote sensing of solar-induced chlorophyll fluorescence: Review of methods and applications. *Remote Sensing of Environment*, *113*, 2037–2051.

Meroni, M., Busetto, L., Colombo, R., Guanter, L., Moreno, J., & Verhoef, W. (2010). Performance of spectral fitting methods for vegetation fluorescence quantification. *Remote Sensing of Environment*, *114*, 363–374 (2010).

Miller, J. R., Berger, M., Alonso, L., Cerovic, Z., Goulas, Y., Jacquemoud, S., et al. (2004). Progress on the development of an integrated canopy fluorescence model, 2003. *International Geoscience and Remote Sensing Symposium, IGARSS'03, vol. 1.* (pp. 601–603) Toulouse (France), 21–25 / 7 /2004. ISBN 0-7803-7929-2 - 0-7803-7930-6.

Mills, T. M., Behboudian, M. H., & Tan, P. Y. (1994). Plant water status and fruit quality in "Braeburn" apples. *Horticultural Science*, *29*, 1274–1278.

Moran, M., Clarke, T., Inoue, Y., & Vidal, A. (1994). Estimating crop water deficit using the relation between surface-air temperature and spectral vegetation index. *Remote Sensing of Environment*, *49*, 246–263.

Moya, I., Camenen, L., Evain, S., Goulas, Y., Cerovic, Z. G., & Latouche, G. (2004). A new instrument for passive remote sensing 1. Measurements of sunlight-induced chlorophyll fluorescence. *Remote Sensing of Environment*, *91*, 186–197.

Papageorgiou, G. (1975). Chlorophyll fluorescence: An intrinsic probe of photosynthesis. In Govindjee (Ed.), *Bioenergetics of photosynthesis* (pp. 319–371). New York: Academic Press.

Pedrós, R., Jacquemoud, S., Goulas, Y., Louis, J., & Moya, I. (2004). *A new leaf fluorescence model, 2nd international workshop on remote sensing of vegetation fluorescence, 17–19 November.* Canada: Montreal.

Pedrós, R., Moya, I., Goulas, Y., & Jacquemoud, S. (2008). Chlorophyll fluorescence emission spectrum inside a leaf. *Photochemical and Photobiological Sciences*, *7*(4), 498–502.

Peguero-Pina, J. J., Morales, F., Flexas, J., Gil-Pelegrín, E., & Moya, I. (2008). Photochemistry, remotely sensed physiological reflectance index and de-epoxidation state of the xanthophyll cycle in *Quercus coccifera* under intense drought. *Oecologia*, *156*(1), 1–11.

Pérez-Priego, O., Zarco-Tejada, P. J., Sepulcre-Cantó, G., Miller, J. R., & Fereres, E. (2005). Detection of water stress in orchard trees with a high-resolution spectrometer through chlorophyll fluorescence *in-filling* of the O_2-A band. *IEEE Transactions on Geoscience and Remote Sensing*, *43*, 2860–2869.

Rougean, J. -L., & Breon, F. M. (1995). Estimating PAR absorbed by vegetation from bidirectional reflectance measurements. *Remote Sensing of Environment*, *51*, 375–384.

Rouse, J. W., Haas, R. H., Schell, J. A., Deering, D. W., Harlan, J. C. (1974). Monitoring the vernal advancement and retrogradation (greenwave effect) of natural vegetation. NASA/GSFC Type III Final Report, Greenbelt, Maryland, p. 371.

Schreiber, U., & Bilger, W. (1987). Rapid assessment of stress effects on plant leaves by chlorophyll fluorescence measurements. In J. D. Tenhunen, & E. M. Catarino (Eds.), *Plant response to stress* (pp. 27–53). Berlin, Germany: Springer-Verlag.

Schreiber, U., Bilger, W., & Neubauer, C. (1994). Chlorophyll fluorescence as a non-intrusive indicator for rapid assessment of in vivo photosynthesis. In E. D. Schulze, & M. M. Caldwell (Eds.), *Ecophysiology of photosynthesis. Ecological Studies*, *vol. 100*. (pp. 49–70) Berlin Heidelberg New York: Springer.

Sepulcre-Cantó, G., Zarco-Tejada, P. J., Jiménez-Muñoz, J. C., Sobrino, J. A., de Miguel, E., & Villalobos, F. J. (2006). Within-field thermal variability detection as function of water stress in *Olea europaea* L. orchards with high spatial remote sensing imagery. *Agricultural and Forest Meteorology*, *136*, 31–44.

Sepulcre-Cantó, G., Zarco-Tejada, P. J., Jiménez-Muñoz, J. C., Sobrino, J. A., Soriano, M. A., Fereres, E., et al. (2007). Monitoring yield and fruit quality parameters in open-canopy tree crops under water stress. Implications for ASTER. *Remote Sensing of Environment*, *107*, 455–470.

Sepulcre-Cantó, G., Zarco-Tejada, P. J., Sobrino, J. A., Berni, J. A. J., Jiménez-Muñoz, J. C., & Gastellu-Etchegorry, J. P. (2009). Discriminating irrigated and rainfed olive orchards with thermal ASTER imagery and DART 3D simulation. *Agricultural and Forest Meteorology*, *149*, 962–975.

Soukupová, J., Cséfalvay, L., Urban, O., Kosvancová, M., Marek, M., Rascher, U., et al. (2008). Annual variation of the steady-state chlorophyll fluorescence emission of evergreen plants in temperate zone. *Functional Plant Biology*, *35*, 63–76.

Suarez, L., Zarco-Tejada, P. J., Sepulcre-Cantó, G., Pérez-Priego, O., Miller, J. R., Jiménez-Muñoz, J. C., et al. (2008). Assessing canopy PRI for water stress detection with diurnal airborne imagery. *Remote Sensing of Environment*, *112*, 560–575.

Suárez, L., Zarco-Tejada, P. J., Berni, J. A. J., González-Dugo, V., & Fereres, E. (2009). Modelling PRI for water stress detection using radiative transfer models. *Remote Sensing of Environment*, *113*, 730–744.

Suárez, L., Zarco-Tejada, P. J., González-Dugo, V., Berni, J. A. J., Sagardoy, R., Morales, F., et al. (2010). Detecting water stress effects on fruit quality in orchards with time-series PRI airborne imagery. *Remote Sensing of Environment*, *114*, 286–298.

Slatyer, J. O. (1967). *Plant–water relationships.* New York and London: Academic press 366p.

Tanner, C. B. (1963). Plant temperatures. *Agronomy Journal*, *55*, 210–211.

Thenot, F., Méthy, M., & Winkel, T. (2002). The photochemical reflectance index (PRI) as a water-stress index. *International Journal of Remote Sensing*, *23*(23), 5135–5139.

Verhoef, W. (2004). *(2005), Extension of SAIL to model solar-induced canopy fluorescence spectra, 2nd international workshop on remote sensing of vegetation fluorescence, 17–19 Nov.* Canada: Montreal.

Villalobos, F. J., Testi, L., & Moreno-Perez, M. F. (2008). Evaporation and canopy conductance of citrus orchard. *Agricultural Water Management*, *96*(4), 565–573.

Vogelmann, J. E., Rock, B. N., & Moss, D. M. (1993). Red edge spectral measurements from sugar maple leaves. *International Journal of Remote Sensing*, *14*, 1563–1575.

Zarco-Tejada, P. J., Miller, J. R., Mohammed, G. H., Noland, T. L., & Sampson, P. H. (2000). Chlorophyll fluorescence effects on vegetation apparent reflectance: II. Laboratory and airborne canopy-level measurements with hyperspectral data. *Remote Sensing of Environment*, *74*(3), 596–608.

Zarco-Tejada, P. J., Miller, J. R., Mohammed, G. H., Noland, T. L., & Sampson, P. H. (2001). Scaling-up and model inversion methods with narrow-band optical indices for chlorophyll content estimation in closed forest canopies with hyperspectral data. *IEEE Transactions on Geoscience and Remote Sensing*, *39*(7), 1491–1507.

Zarco-Tejada, P. J., Berjón, A., López-Lozano, R., Miller, J. R., Marin, P., Cachorro, V., et al. (2005). Assessing vineyard condition with hyperspectral indices: Leaf and canopy reflectance simulation in a row-structured discontinuous canopy. *Remote Sensing of Environment*, *99*, 271–287.

Zarco-Tejada, P. J., Miller, J. R., Pedrós, R., Verhoef, W., & Berger, M. (2006). FluorMODgui V3.0 — A graphic user interface for the leaf and canopy simulation of chlorophyll fluorescence. *Computers & Geosciences*, *32*(5), 577–591.

Zarco-Tejada, P. J., Berni, J. A. J., Suárez, L., & Fereres, E. (2008). A new era in remote sensing of crops with unmanned robots. *SPIE Newsroom*, doi:10.1117/2.1200812.1438.

Zarco-Tejada, P. J., Berni, J. A. J., Suárez, L., Sepulcre-Cantó, G., Morales, F., & Miller, J. R. (2009). Imaging chlorophyll fluorescence from an airborne narrow-band multispectral camera for vegetation stress detection. *Remote Sensing of Environment*, *113*, 1262–1275.